LEVEL III

DNA 4818F

STATISTICAL BEHAVIOR OF SIGNALS FROM THE WIDEBAND SATELLITE

Physical Dynamics, Inc.
P.O. Box 3027
Bellevue, Washington 98009

31 December 1978

Final Report for Period 15 November 1977—31 December 1978

CONTRACT No DNA 001-78-C-0042

APPROVED FOR PUBLIC RELEASE;
DISTRIBUTION UNLIMITED.

THIS WORK SPONSORED BY THE DEFENSE NUCLEAR AGENCY
UNDER RDT&E RMSS CODE B322078462 I25AAXYX96014 H2590D.

Prepared for
Director
DEFENSE NUCLEAR AGENCY
Washington, D. C. 20305

Destroy this report when it is no longer needed. Do not return to sender.

PLEASE NOTIFY THE DEFENSE NUCLEAR AGENCY, ATTN: STTI, WASHINGTON, D.C. 20305, IF YOUR ADDRESS IS INCORRECT, IF YOU WISH TO BE DELETED FROM THE DISTRIBUTION LIST, OR IF THE ADDRESSEE IS NO LONGER EMPLOYED BY YOUR ORGANIZATION.

UNCLASSIFIED

SECURITY CLASSIFICATION OF THIS PAGE *(When Data Entered)*

REPORT DOCUMENTATION PAGE	READ INSTRUCTIONS BEFORE COMPLETING FORM
1. REPORT NUMBER: DNA 4818F	2. GOVT ACCESSION NO.: AD-A084 646
3. RECIPIENT'S CATALOG NUMBER:	
4. TITLE *(and Subtitle)*: STATISTICAL BEHAVIOR OF SIGNALS FROM THE WIDEBAND SATELLITE	5. TYPE OF REPORT & PERIOD COVERED: Final Report for Period 15 Nov 77—31 Dec 78
	6. PERFORMING ORG. REPORT NUMBER: PD-NW-79-193R
7. AUTHOR(s): Edward J. Fremouw, Deborah A. Miller	8. CONTRACT OR GRANT NUMBER(s): DNA 001-78-C-0042
9. PERFORMING ORGANIZATION NAME AND ADDRESS: Physical Dynamics, Inc., P.O. Box 3027, Bellevue, Washington 98009	10. PROGRAM ELEMENT, PROJECT, TASK AREA & WORK UNIT NUMBERS: Subtask I25AAXYX960-14
11. CONTROLLING OFFICE NAME AND ADDRESS: Director, Defense Nuclear Agency, Washington, D.C. 30205	12. REPORT DATE: 31 December 1978
	13. NUMBER OF PAGES: 60
14. MONITORING AGENCY NAME & ADDRESS*(if different from Controlling Office)*:	15. SECURITY CLASS *(of this report)*: UNCLASSIFIED
	15a. DECLASSIFICATION/DOWNGRADING SCHEDULE:

16. DISTRIBUTION STATEMENT *(of this Report)*

Approved for public release; distribution unlimited.

17. DISTRIBUTION STATEMENT *(of the abstract entered in Block 20, if different from Report)*

18. SUPPLEMENTARY NOTES

This work sponsored by the Defense Nuclear Agency under RDT&E RMSS Code B322078642 I25AAXYX96014 H2590D.

19. KEY WORDS *(Continue on reverse side if necessary and identify by block number)*

Plasma-Density Striations
Scattering of Electromagnetic Waves
Scintillation of Complex Signals
Signal Statistics
Transionospheric Communications

20. ABSTRACT *(Continue on reverse side if necessary and identify by block number)*

Optical and radio signals that have been scattered by random refractive-index structure must be described statistically in systems-oriented codes and other applications. The general nature of the statistics that would best describe such signals has been an open question for some time, with different models being used close to the medium (log-normal) and far from it (Rician). Signal behavior in the intermediate zone, which is the relevant distance regime for radiowave communication through the structured ionosphere and through

DD FORM 1 JAN 73 1473 EDITION OF 1 NOV 65 IS OBSOLETE

UNCLASSIFIED

SECURITY CLASSIFICATION OF THIS PAGE *(When Data Entered)*

20. ABSTRACT (Continued)

striated, high-altitude nuclear plasmas, has been difficult to characterize in a general and systematic way. The Wideband satellite experiment, with its multiple, coherent frequencies and its variety of observing geometries, has provided a wealth of data upon which to base a general model.

In this work, careful and detailed analysis has been performed of VHF, UHF, and L-band data from the Wideband receiving stations at Ancon, Kwajalein, Stanford, and Poker Flat to establish the statistical behavior of scattered signals over a wide range of scattering strength, Fresnel-zone size (which sets the effective distance), and scattering geometry. Histograms of intensity and phase were compared, by means of chi-square testing, with probability density functions derived from four leading signal-statistical hypotheses: log-normal; generalized Gaussian, of which Rice statistics are a special case; two-component, which invokes the log-normal and generalized Gaussian hypotheses in different regimes of the signal fluctuation spectrum; and Nakagami-m, which is an approximation to generalized Gaussian statistics addressing only the behavior of signal intensity.

The analysis disclosed the expected efficacy of log-normal statistics in the near zone, limited to conditions of weak intensity scintillation, and a tendency toward generalized-Gaussian statistics approaching the far zone, limited to a modulo-2π description of phase. It clearly demonstrated, however, that log-normal statistics do not provide a generally valid description of intensity scintillation and that the generalized-Gaussian model does not characterize the overall behavior of complex-signal scintillation. The two-component model was found to be generally efficacious for describing all aspects of signal behavior in all regimes, providing a systematic transition between the two classical models.

A strong conclusion has been reached in support of the Nakagami-m distribution as a general descriptor of intensity fading and of the normal distribution as an indicator of phase behavior, the first-order statistics of which usually are altered little in post-scattering propagation. At present, there is no underlying signal-statistical hypothesis that leads to both joint Nakagami-normal behavior and an accounting for correlation between intensity and phase fluctuations, which is commonly observed. It is suggested that such an hypothesis be formulated inductively and tested empirically. Meanwhile, the Nakagami-m distribution can be used confidently to describe intensity behavior and the normal distribution to describe phase behavior. For a full description of the joint statistics of intensity and phase, at present, one must employ the two-component model, which requires six moments for its specification. A joint Nakagami-normal model would require only three moments, two of which are the commonly employed intensity and phase scintillation indices.

The analysis reported herein also elucidates the manner in which radio-wave observations and/or communication transmissions of finite duration impose an effective outer scale on a scattering medium observed in the intermediate zone. For anisotropic scatterers, the imposed outer scale is highly geometry-dependent, requiring caution in extrapolating experimental results to disparate operational situations. It is demonstrated that presently available propagation theory does provide the tools necessary for proper extrapolation.

TABLE OF CONTENTS

LIST OF FIGURES

LIST OF FIGURES (Continued)

LIST OF TABLES

I. INTRODUCTION

A. BACKGROUND

The statistical behavior of an electromagnetic signal that has propagated through a random medium has been investigated by workers in several related fields. A general solution to the problem is of interest as a scientific challenge to understand wave-medium interactions, and identification of specific signal-statistical characteristics has been sought for application both to remote sensing of various propagation media and to the efficient transmission of information through them.

The most direct theoretical attacks on problems of signal statistics involve moment calculations for the distribution of one or more observables, such as the electromagnetic wave's quadrature components or intensity and phase (Hewish, 1951; Bramley, 1955; Bowhill, 1961; Yeh, 1962; Uscinski, 1967; Strohbehn, 1968; Barabenenkov et al, 1971; Tatarskii, 1971; de Wolf, 1972; Fante, 1975; Ishimaru, 1975; Rino, 1976). Applications range from radio astronomy (Salpeter, 1967; Lovelace et al, 1970; Valley and Knepp, 1976) and ionospheric physics (Fremouw and Lansinger, 1968; Crane, 1976) to atmospheric remote sensing (Beard, Kreiss, and Tank, 1969; Furuhama and Fukushima, 1973) and both optical and radio transmission (Ochs, Bergman, and Snyder, 1969; Gurvich and Tatarskii, 1975; Fremouw and Rino, 1978).

Only in special circumstances (e.g., in the Fraunhoffer diffraction zone of a medium containing refractive-index irregularities with an effective outer scale) have sufficient moment calculations been carried out (e.g., Mercier, 1962) to completely define the first-order distribution of the complex signal (e.g., Rician). In other circumstances, only numerical (Buckley, 1975) and empirical (Knepp and Valley, 1978) approaches are tractable. Moreover, the vast majority of theoretical work and much of the experimental effort has centered on the statistics of signal intensity (e.g., Rino, Livingston, and Whitney, 1976) because phase calculations are difficult and phase references often are not available in experiments.

In the work reported here, a direct experimental attack has been made on identifying the underlying statistics that characterize the joint behavior of the intensity and phase of a (radio) signal that has undergone narrow-angle forward scattering in a remote (ionospheric) region containing (real) refractive-index irregularities with an effectively infinite outer scale and an effectively zero inner scale. The data employed were obtained by means of the DNA-002 Wideband coherent satellite beacon, which transmits ten mutually coherent signals ranging in frequency from VHF through S band. The signals were recorded at ground stations located in the auroral, mid-latitude, and equatorial zones.

Historically, there have been two heuristic views of the manner in which signal perturbations develop due to interactions of a wave with a random medium. The first is based on the mental picture of a wave propagating in essentially straight paths along which the phase, ϕ, is randomly increased and decreased, differently on different paths. Applying the central limit theorem to the random walk undergone by the phase in traversing the medium leads to an expectation that the phase will be a Gaussian variate (e.g., Bramley, 1955). A natural extension of this construction, which is particularly convenient for application of the Rytov (1937) perturbation technique, is to suppose that the real and imaginary parts of the logarithm of the signal are normal variates, so that the intensity obeys a log-normal distribution (Strohbehn and Wang, 1972).

Close to the medium, the foregoing "multiplicative" (Strohbehn, Wang, and Speck, 1975) model (so-named because the complex phasor, E, representing the wavefield is perturbed by multiplicative effects in adjacent slabs of the medium) is satisfactory even when multiple scatterings lead to strong phase perturbations. It becomes suspect (Wang and Strohbehn, 1974a), however, whenever significant fluctuations in wave intensity, I, develop (even for moderate phase fluctuation) through the effect of propagation, because its attendant perturbation technique for calculating E breaks down.

The alternate historical view leads to the "additive" (Strohbehn, Wang, and Speck, 1975) model, in which component phasors are added and the central limit theorem is applied to the real, x, and imaginary, y, parts of E rather than of its logarithm. Far from the scattering medium, where propagation has produced a uniform distribution (modulo 2π) of random phases among the elemental wavelets, the resultant wavefield clearly obeys Rice (1945) statistics, reducing to Rayleigh statistics for sufficiently strong (in the aggregate) scatter.

Close to the medium and for sufficiently weak scatter, an identification can be made between the phase perturbations imposed by the medium and fluctuations in the imaginary part of E. Propagation calculations based on the first Born approximation then yield the second moments needed to characterize the generalized bivariate Gaussian distribution of x and y. The identification of y with ϕ, and of x with $\sqrt{I}$, however, clearly breaks down for strong scatter, even close to the medium.

For very weak scatter, the multiplicative and additive views lead to the same results since fluctuations in E and in its logarithm then are virtually identical. Recapping, we find (1) that the multiplicative model is satisfactory for any degree of scatter close to the medium but becomes decreasingly satisfactory with increasing distance for moderate to strong scatter; (2) that the additive model is satisfactory for any degree of scatter far from the medium but becomes decreasingly satisfactory with decreasing distance for moderate

to strong scatter; and (3) that either model will suffice for very weak scatter at any distance.

Regimes of validity for various signal-statistical calculations have been laid out systematically by de Wolf (1969, 1975) for observations inside an extended medium. His "saturation" zone corresponds approximately to the region identified heuristically above as not being well described by either the multiplicative or the additive model -- namely, the middle-distance regime for moderate and strong scatter. A closely related ordering of regimes has been presented by Singleton (1970) for observations not necessarily within the medium, although for a medium characterized by a single scale (Gaussian spatial spectrum). Both these orderings, however, address only intensity statistics, whereas the present work deals with complex-signal statistics. The latter also deals directly with "middle" distances in which the Fresnel radius lies between the inner and outer scales of a power-law scattering medium, both scales in fact lying outside the spectral window filled by the data available.

B. OBJECTIVE

There have been two essential approaches to obtaining a general description of the signal statistics arising from scattering. The first is to seek an approximate analytical solution, guided by experiment, to the general problem of defining a relevant distribution function. Nakagami (1960) has summarized a remarkably tenacious and quite productive series of attacks on the problem in Japan, limited however to description of intensity statistics. The second approach is to combine the multiplicative and additive models in such a way as to provide a generally useful hybrid distribution. Workers in the optics (Wang and Strohbehn, 1974b) and radio (Fremouw, Rino, and Livingston, 1976) communities have independently proposed very similar hybrid models, the latter being somewhat more general but requiring more parameters for its definition.

The main objective of the present work is to establish the relative utility of the four leading signal-statistical models -- multiplicative (log-normal), additive (in its generalized Gaussian form), approximate (Nakagami-m), and hybrid (general two-component) -- for describing the behavior of radio waves that have undergone narrow-angle forward scatter in a structured plasma. The approach, which is described in Section II, was to perform hypothesis testing by means of chi-square evaluation of distribution functions for phase and intensity, employing observations of the complex signal received from a satellite transmitting through the ionosphere; the results of hypothesis testing are presented in Section III A. Insight gained into the parameter relationship between phase and intensity fluctuations (scintillations) are described in Section III B, and conclusions drawn from the work are presented in Section IV.

II. EXPERIMENTAL APPROACH

A. DATA EMPLOYED

In May of 1976, satellite P76-5 was launched into a near-circular (1000 km), high-inclination (99.7°), sun-synchronous (equator crossings at about 1120 and 2320, local time) orbit with the DNA-002 Wideband beacon as its sole payload. The Wideband beacon transmits ten mutually coherent CW signals, ranging from VHF (138 MHz) through UHF (seven spectral lines centered at 413 MHz and equally spaced 11.5 MHz apart) to L band (1239 MHz) and S band (2891 MHz), for the purpose of diagnosing the transionospheric radio communication channel and describing the plasma-density irregularities that perturb it. Observations of dispersion (interpreted as ionospheric total electron content) and complex-signal scintillation at the nine lowest frequencies, employing the S-band signal as an essentially unperturbed phase reference, have been conducted at auroral, mid-latitude, and equatorial stations.

In the present assessment of (first-order) complex-signal statistics, recordings of scintillating VHF, UHF, and L-band signals obtained at Poker Flat, Alaska (65.4° magnetic dip latitude), Ancon, Peru (0.4° dip latitude), Kwajalein, Marshall Islands (4.4° dip latitude), and Stanford, California (42.8° dip latitude) have been employed. The quadrature components of each signal were recorded at a rate of 500 samples per second, after passing through low-pass filters having bandwidths of 150 Hz, throughout satellite passes of many minutes duration. The data employed in this analysis were decimated to 100 samples per second, converted to intensity and phase, and detrended to remove Fourier periods greater than 10 seconds (Fremouw et al, 1978). The data window for intensity and phase, therefore, corresponds to a spatial spectrum (as the line of sight scanned through the F layer) between wavelengths of approximately 60 meters and 30 km. It appears, both from these data and other experimental results (e.g., Dyson, McClure, and Hanson, 1974), that the data window employed consistently fell between the inner and outer scales of ionospheric structure.

B. SIGNAL-STATISTICAL HYPOTHESES

1. Single-Component Models:

The data processing employed included calculation of relevant statistical moments, computation of various signal spectra useful for assessing propagation effects, plots of time series for data-quality control, and calculation of chi-square fits for evaluation of four signal-statistical hypotheses: log-normal, generalized Gaussian, Nakagami-m, and two-component. The log-normal model is defined by the hypothesis that the real and imaginary parts of the complex logarithm of the received signal are jointly normal variates.

That is, if the complex voltage output from the receiving antenna at a given radio frequency is

$$E = A\, e^{i\phi} = \exp(\chi + i\phi) \tag{1}$$

then the joint probability density function (pdf) of χ and ϕ is

$$p_n(\chi,\phi) = \frac{1}{2\pi\sigma_\chi \sigma_\phi (1-\rho^2_{\chi\phi})^{\frac{1}{2}}} \exp\left[- \frac{\sigma_\phi^2 (\chi - \langle\chi\rangle)^2 - 2\sigma_\chi \sigma_\phi \rho_{\chi\phi} (\chi - \langle\chi\rangle)\phi + \sigma_\chi^2 \phi^2}{2\sigma_\chi^2 \sigma_\phi^2 (1-\rho^2_{\chi\phi})} \right] \tag{2}$$

where $\langle\chi\rangle$ is the mean value of χ, σ_χ and σ_ϕ are the standard deviations of χ and ϕ respectively, and $\rho_{\chi\phi}$ is the correlation coefficient between χ and ϕ. The mean value of ϕ is taken as the phase reference and therefore is zero by definition.

Under postulate (2), the individual pdf's of intensity ($I=A^2$) and phase are respectively the following log-normal and normal functions:

$$p_I(I) = \frac{1}{2\sqrt{2\pi}\sigma_\chi I} \exp\left\{ \frac{-[\ln I - 2\langle\chi\rangle]^2}{8\sigma_\chi^2} \right\} \tag{3}$$

$$p_n(\phi) = \frac{1}{\sqrt{2\pi}\sigma_\phi} \exp\left(\frac{-\phi^2}{2\sigma_\phi^2} \right) \tag{4}$$

So-called Gaussian signal statistics follow from the hypothesis that the real and imaginary parts of the antenna voltage itself, rather than of its logarithm, are jointly normal variates. That is, given

$$E = A\, e^{i\phi} = x + iy \tag{5}$$

then the joint pdf of x and y is

$$p_G(x,y) = \frac{1}{2\pi\sigma_x\sigma_y(1-\rho^2_{xy})^{\frac{1}{2}}} \exp\left[- \frac{\sigma_y^2 (x - \langle x\rangle)^2 - 2\sigma_x \sigma_y \rho_{xy} (x - \langle x\rangle)y + \sigma_y^2 y^2}{2\sigma_x^2 \sigma_y^2 (1-\rho^2_{xy})} \right] \tag{6}$$

The mean, variances, and correlation coefficient in Eq. (6) are analogous to those in Eq. (2), but they are calculated from the outputs of a pair of quadrature detectors rather than from the result of envelope and phase detection.

In the general case of Gaussian statistics represented by Eq. (6), the individual pdf's for intensity and phase are considerably more complicated than Eqs. (3) and (4).

Indeed, the intensity pdf is obtainable only by numerical integration (Fremouw and Rino, 1975) or in terms of an infinite series (Beckman and Spizzichino, 1963). Hatfield, however, has succeeded in obtaining the following analytic expression for the phase pdf (Hatfield and Rino, 1975):

$$P_H(\phi) = \frac{\sigma_x \sigma_y (1-\rho_{xy}^2)^{\frac{1}{2}}}{2\pi D} \exp\left[\frac{-\langle x\rangle^2 \sigma_y^2}{2\sigma_x^2\sigma_y^2(1-\rho_{xy}^2)}\right]$$

$$+ \frac{\langle x\rangle \sigma_x \sigma_y E}{2\sqrt{2\pi} D^{3/2}} \exp\left\{-\left[\frac{\langle x\rangle^2 \sigma_y^2 (1+E\sigma_x^2/D)}{2\sigma_x^2\sigma_y^2(1-\rho_{xy}^2)}\right]\right\} \operatorname{erfc}\left[\frac{-\langle x\rangle \sigma_x \sigma_y E}{\sqrt{2D}\,\sigma_x\sigma_y(1-\rho_{xy}^2)^{\frac{1}{2}}}\right] \tag{7}$$

where $D = \sigma_y^2 \cos^2\phi - 2\rho_{xy}\sigma_x\sigma_y \cos\phi \sin\phi + \sigma_x^2 \sin^2\phi$ (8)

and $E = \sigma_y^2 \cos\phi - \rho_{xy}\sigma_x\sigma_y \sin\theta.$ (9)

While the pdf's for intensity and phase are very complicated in the general case of Gaussian statistics, they reduce to quite familiar forms for certain special cases. For instance, the case in which x and y have equal variances (σ_x^2 and σ_y^2) and are uncorrelated ($\rho_{xy} = 0$) produces the well-known Rice statistics obeyed by a steady signal accompanied by noise. When the noise totally dominates the signal ($\sigma_x^2 + \sigma_y^2 = \langle I\rangle$), we have Rayleigh statistics.

A more general approximation to Gaussian statistics has been worked out by Nakagami (1960) by means of a semi-empirical procedure. The so-called Nakagami-m distribution for intensity, which approaches the Rice distribution as m approaches unity from above and equals the Rayleigh distribution when m = 1, is

$$P_N(I) = \frac{m^m I^{m-1}}{\Gamma(m)\langle I\rangle^m} e^{-mI/\langle I\rangle} \tag{10}$$

where

$$m \triangleq \frac{\langle I\rangle^2}{\langle I^2\rangle - \langle I\rangle^2} \triangleq \frac{1}{S_4^2} \tag{11}$$

The Nakagami distribution has attained considerable favor among observers of intensity scintillation (Whitney, 1974), since it is independent of any phase-related parameter. By the same token, there is no phase pdf accompanying the Nakagami distribution, nor is there a related description of the joint statistics of intensity and phase.

2. Two-Component Model:

Even the generalized Gaussian statistics yield only a limited description of phase.

The Hatfield distribution, for instance, is defined only modulo 2π and is therefore of limited value under the common scintillation condition in which phase variations exceed $\pm\pi$, as we shall see. This limitation is overcome, as a practical matter, in two-component signal-statistical models. The two-component model tested in the present work is that put forth by Fremouw, Rino, and Livingston (1976), in which the total scintillating signal, E, is modeled as the product of a diffractively scattered component, E_s, and a refractively focused component, E_f, such that

$$E = A\, e^{i\phi} = E_s E_f = (x_s + iy_s)\exp(\chi_f + i\phi_f). \tag{12}$$

In this two-component model, it is postulated that E_s obeys generalized Gaussian statistics [Eq. (6)] and that E_f obeys log-normal statistics [Eq. (2)]. A heuristic rationale for the two-component model can be made by considering a wave that passes through a region of large-scale, phase-perturbing structure and then through a layer of smaller-scale scatterers. The phase of the wave would have undergone a random walk through the first region, and weak focuses and defocuses would develop in subsequent propagation. It is postulated that this process leads to log-normal statistics.

Upon passing through the second layer, the wave would emerge with a scattered (coherent) and a non-scattered (noncoherent) part. The latter would retain log-normal statistics, but the former would be disrupted by the diffraction process, leading to Gaussian statistics. A tacit assumption in the two-component model is that the resulting statistics are independent of whether the small-scale scatter takes place before, after, or concurrently with the large-scale phase perturbations. The two components are taken to be multiplicative because signal components behaving qualitatively as those postulated in the model were isolated by means of a coherent-AGC process which is tantamount to dividing E by E_f, as illustrated by Fremouw et al (1978).

A basic postulate in the two-component model is that E_s and E_f are statistically independent. Experimentally, this is ensured by isolating the two components by means of a very sharp filter (a ten-pole Butterworth in the present work). In terms of propagation theory, this experimental step corresponds to a partitioning of the scattering medium in such a way that the scale for changes in the transverse gradient of $\ln E_f$ are much larger than the scale for changes in the transverse gradient of E_s. Under such a partitioning, the parabolic wave equation can be solved independently for the two components, as has been carried out by Rino (Fremouw and Rino, 1978).

Under the postulate of statistical independence, it is straightforward to show that

$$\langle E \rangle = \langle x_s \rangle \exp\left(\langle \chi_f \rangle + B_f/2\right) \tag{13}$$

$$\langle EE^* \rangle = (\langle x_s \rangle^2 + \sigma_s^2) \exp\left(\langle \chi_f \rangle + \sigma_{\chi_f}^2\right) \equiv 1 \tag{14}$$

$$\text{and} \quad \langle EE \rangle = (\langle x_s \rangle^2 + B_s) \exp\left[2\langle \chi_f \rangle + B_f\right] \tag{15}$$

$$\text{where} \quad B_f \triangleq \sigma_{\chi_f}^2 - \sigma_{\phi_f}^2 + 2i\rho_{\chi_f\phi_f}\sigma_{\chi_f}\sigma_{\phi_f} \tag{16}$$

$$\sigma_s^2 \triangleq \sigma_{x_s}^2 + \sigma_{y_s}^2 \tag{17}$$

$$\text{and} \quad B_s \triangleq \sigma_{x_s}^2 - \sigma_{y_s}^2 + 2i\rho_{x_s y_s}\sigma_{x_s}\sigma_{y_s} \tag{18}$$

and where we have used the fact that the experimental separation of E_s and E_f results approximately in $\langle y_s \rangle \approx \langle \phi_f \rangle = 0$ and where conservation of energy is invoked as the normalization condition [Eq. (14)]. It also follows that

$$\langle \phi^2 \rangle = \langle \phi_f^2 \rangle + \left\langle \left(\tan^{-1} \frac{y_s}{x_s} \right)^2 \right\rangle \tag{19}$$

$$\text{and} \quad S_4^2 = \left[(S_4^2)_s + 1\right]\left[(S_4^2)_f + 1\right] - 1 \tag{20}$$

where $(S_4)_{s,f}$ are the component intensity scintillation indices [defined according to Eq. (11)].

Cursory inspection of Eq. (20) might suggest that the two-component model predicts occurrence of S_4 values considerably in excess of unity (for instance, $S_4 = \sqrt{3}$ for $S_{4s} = S_{4f} = 1$). While the model would admit such a situation, it does not in fact predict it since it does not address the question of a parameter dependence between S_{4s} and S_{4f}. The largest value of S_4 yet observed in the Wideband experiment is 1.2, and detailed inspection of signal behavior suggests that only the coherent part of E_s may be susceptible to significant focusing and defocusing, which would put a limit on simultaneously large (near unity) values of S_{4s} and S_{4f}.

For purposes of hypothesis testing, we need the pdf's for phase and intensity under the two-component model. For phase, the problem is trivial because $\phi = \phi_f + \phi_s$, where $\phi_s \triangleq \tan^{-1}(y_s/x_s)$ and where ϕ_f and ϕ_s are statistically independent. Thus, the pdf for the composite phase is the following convolution:

$$p_{c\phi}(\phi) = \int_{-\infty}^{\infty} p_H(\phi_s)\, p_n(\phi - \phi_s)\, d\phi_s \tag{21}$$

where p_H is the Hatfield distribution [Eq. (7)] and p_n is the normal distribution [Eq. (4)].

Similarly, from the statistical independence of χ_f and χ_s ($\triangleq \frac{1}{2} \ell n\, I_s$), one can show, by means of a series of coordinate transformations, that the pdf for the composite intensity in the two-component model is

$$p_{cI}(I) = \int_{-\infty}^{\infty} I_s^{-1} p_{GI}(I_s) p_\ell \left(\frac{I}{I_s}\right) dI_s \tag{22}$$

where $I_s = x_s^2 + y_s^2$ and where p_{GI} is the intensity pdf arising from numerical integration of Eq. (6) and p_ℓ is the log-normal pdf defined in Eq. (3).

More than just the individual pdf's, however, the two-component hypothesis provides a joint distribution for intensity and phase. Employing reasoning similar to that leading to Eqs. (21) and (22) and invoking statistical independence of the two components, one finds the following joint pdf:

$$p_c(I,\phi) = \frac{1}{2I} \int\int_{-\infty}^{\infty} e^{2\chi_s} p_G(e^{\chi_s}\cos\phi_s, e^{\chi_s}\sin\phi_s) p_n(\tfrac{1}{2}\ell nI - \chi_s, \phi - \phi_s) d\chi_s\, d\phi_s \tag{23}$$

which is essentially a two-dimensional convolution of the two bivariate normal distributions defined in Eqs. (2) and (6).

C. DATA PROCESSING

1. Sample Selection:

To obtain a representative set of data samples for detailed signal-statistical analysis, the entire collection of (singly) detrended VHF strip charts (cf, Figure 6 of Fremouw et al, 1978) obtained during approximately the first year of the Wideband experiment was inspected. The inspection was aimed at obtaining about one hundred data samples of at least 20 seconds duration during which the received signals displayed reasonable statistical stationarity. Selection criteria included an attempt to find samples reasonably well distributed in satellite elevation angle and scintillation disturbance level and to have representation from all four receiving stations: Ancon, Kwajalein, Poker Flat, and Stanford.

Table 1 shows the distribution of record segments selected (ranging in duration from 20 to 85 seconds), for all of which VHF data were processed. For the more disturbed segments, meaningful analysis could be conducted at higher frequencies, and the number of VHF, UHF, and L-band data segments analyzed from each station is given in Table 2.

Table 1. Distribution of VHF dual-detrend data sets processed

Location	Elevation	Disturbance level Weak	Moderate	Strong
Ancon	Low (<20°)	1		2
	Medium (20-50°)	1	1	4
	High (>50°)			3
Kwajalein	Low (<20°)	2	3	5
	Medium (20-50°)	4	5	3
	High (>50°)		1	
Poker Flat	Low (<20°)	1	1	1
	Medium (20-50°)	2	5	2
	High (>50°)		2	1
Stanford	Low (<20°)	1	3	3
	Medium (20-50°)	1	3	
	High (>50°)		1	

Table 2. Number of dual-detrend data sets processed

Location	VHF	UHF	L-band	Total
Ancon	12	9	6	27
Kwajalein	23	11	4	38
Poker Flat	15	6	4	25
Stanford	12	4		16
	62	30	14	106

2. The Dual-Detrend Processor:

Under this contract, the dual detrending procedure developed by Fremouw and Livingston (1976) was employed for analysis of the data sets summarized in Tables 1 and 2, in order to test the two-component hypothesis and the three single-component hypotheses. The processor also provides a wealth of complementary information on signal behavior, performing numerous computational functions and delivering several numerical and graphical outputs.

Central to the processing performed is computation of a number of first-order, signal-statistical moments. For the composite (ie, 0.1-Hz singly detrended) signal, the following moments are computed: the mean intensity, $\langle I \rangle$; the mean log-amplitude, $\langle \chi \rangle$; the mean real and imaginary parts, $\langle x \rangle$ and $\langle y \rangle$ (≈ 0); the normalized standard deviation of intensity, S_4; the standard deviation of log-amplitude, σ_χ; the standard deviation of phase, σ_ϕ; the variances of the real and imaginary parts, σ_x^2 and σ_y^2; the total signal variance, $\sigma_t^2 = \sigma_x^2 + \sigma_y^2$; and various combinations of these moments.

For use in testing the two-component model, several analagous quantities are computed for each of the two components, which are separated by independently passing the composite phase and log-amplitude through a low-pass, ten-pole Butterworth filter having a 3-dB cutoff at 0.4 Hz, storing the results, and then subtracting them from their nonfiltered counterparts. The smoothed results comprise

$$E_f = \exp(\chi_f + i\phi_f) \triangleq \exp(\hat{\chi} + i\hat{\phi}) \tag{24}$$

where $\hat{}$ denotes the smoothing process, and the residuals comprise

$$E_s = x_s + iy_s \triangleq \exp\left[(\chi - \hat{\chi}) + i(\phi - \hat{\phi})\right]. \tag{25}$$

The component moments computed include the following "six sigmas" needed to define the component pdf's: $\sigma_{\chi f}$, $\sigma_{\phi f}$, $\sigma_{\chi f \phi f} = \sqrt{\rho_{\chi f \phi f}\, \sigma_{\chi f}\, \sigma_{\phi f}}$; σ_{xs}, σ_{ys}, $\sigma_{xsys} = \sqrt{\rho_{xsys}\, \sigma_{xs}\, \sigma_{ys}}$. In addition, quantities derived from the six sigmas, such as those defined in Eq. (16), (17), and (18), are calculated for comparison of signal behavior with that predicted by the two-component model, such as that described by Eqs. (13), (14), and (15).

Second-order moments of the composite signal, in the form of several spectra and autocorrelation functions, are computed and output graphically. Specifically, plots are obtained of the power spectra and autocorrelation functions of intensity, I and phase, ϕ, and of the two-sided (positive and negative frequencies) Doppler-spread power spectrum of the received signal, E. Since the signal fluctuations recorded arise from scanning of a

complex diffraction pattern across the receiving antenna, the Doppler spectrum also may be viewed as a one-dimensional cut through the two-dimensional angular spectrum of plane waves arriving at the ground (Booker, Ratcliffe, and Shinn, 1950).

Hypothesis testing is carried out by forming histograms of intensity and phase, separately, from the (composite) complex signals recorded and then comparing the histograms with pdf's computed on the basis of the four signal-statistical hypotheses. The theoretical pdf's are calculated from the relevant moments computed from each data set. For testing the log-normal hypothesis, $\langle\chi\rangle(\neq 0)$ and σ_χ are inserted in Eq. (3), and σ_ϕ is employed in Eq. (4). For testing the generalized Gaussian hypothesis, $\langle x\rangle$, σ_x, σ_y, and ρ_{xy} are used in Eqs. (7), (8), and (9), and Eq. (6) is integrated numerically to obtain $p_{GI}(I)$ from the same moments. (Note that the normalization condition reduces the number of parameters to three, since $\langle x\rangle^2 = \sigma_x^2 + \sigma_y^2$.)

The Nakagami distribution is calculated from Eqs. (10) and (11), employing the observed intensity's mean, $\langle I\rangle$ (=1 by normalization) and variance, $\langle I^2\rangle$. For testing the two-component model, the six sigmas defined after Eq. (25) are employed to calculate the component distributions appearing in Eqs. (21) and (22), and the convolutions are carried out numerically.

For visual comparison, the intensity and phase histograms and the theoretical pdf's are output graphically. Quantitative hypothesis testing, however, is performed by calculating the chi-square difference between each histogram and each corresponding theoretical pdf. An additional graphical output gives a comparison of the histograms of χ_f, ϕ_f, x_s, and y_s with normal curves computed from the relevant means and standard deviations. No quantitative use is made however, of this information about the components of the two-component model.

III. RESULTS

A. HYPOTHESIS TESTS

1. Chi-Square Values

Complete dual-detrend processing, including chi-square testing of the four signal-statistical hypotheses, was conducted on 101 of the 106 data samples enumerated in Table 2. (The other five were processed as test cases during software development, before the chi-square-test routine was operational.) With a few individual exceptions (mainly involving software limitations in generating the Nakagami-m pdf for extremely small S_4), valid chi-square tests were obtained for all distributions. In this section, we present and discuss the behavior of χ^2 as an indicator of the efficacy of the four signal-statistical models.

While it is to be hoped that a single model can be employed for all observing conditions, one might expect to find differences. Accordingly, the test results have been grouped for comparison by observing station and frequency. One might also expect geometrical differences (e.g., a trend with elevation angle), but the geometrical situation is sufficiently complicated that a simple sorting of χ^2 probably would not be productive. Geometrical effects do play an important part in establishing the moments (e.g., the phase and intensity scintillation indices, σ_ϕ and S_4) by which the signal statistics are parameterized, and this effect will be explored in Section III B.

Table 3 gives the mean values and standard deviations of χ^2 for the various models for each of the four stations and three observing frequencies. (VHF is 138 MHz; UHF includes measurements at both 379 and 413 MHz; and L-band is 1239 Mhz.) The numbers in square brackets preceding each mean value indicate the ranking of the model in that column for the data sets in that row. (I.e., [1] denotes the smallest mean χ^2, [2] the next smallest, and so forth.)

Close examination of Table 3 reveals several aspects of the signal-statistical behavior of scintillating complex signals. Let us peruse it first for trends with frequency. Taking note of the model rankings for phase, we find that for no station does the ranking change in going from VHF to UHF, nor does it change at Ancon in going to L-band. The differences observed between the various mean χ^2 values for L-band at Kwajalein are very small, compared with the corresponding standard deviations, and those at Poker Flat are only slightly less so. (Furthermore, the L-band data segments from Kwajalein and Poker Flat represent only 7% of the total population.)

We conclude that there is no statistically significant change in the ranking of phase-statistical models with changing frequency (and, therefore, with changing Fresnel-zone size). As had been inferred earlier (Fremouw et al, 1978) from the frequency dependence of σ_ϕ, which is essentially independent of Fresnel-zone size in most cases, the first-order

Table 3. Means and standard deviations of χ^2
([n] denotes ranking)

	Frequency (No. of χ^2 Values)	Log-Normal	Generalized Gaussian	Two-Component	Nakagami-m
ANCON	VHF (12)				
	Phase	[1] 5.41±6.46	[3] 25.06±12.53	[2] 6.29±6.77	
	Intensity	[4] 104.46±99.20	[2] 7.87±5.83	[3] 14.38±10.96	[1] 7.11±5.36
	UHF (9)				
	Phase	[1] 3.26±1.69	[3] 10.02±9.82	[2] 3.68±2.07	
	Intensity	[3] 39.11±31.88	[4] 45.19±53.16	[1] 8.90±5.59	[2] 9.13±6.18
	L-band (6)				
	Phase	[1] 3.43±1.82	[3] 4.87±2.24	[2] 3.93±1.99	
	Intensity	[1] 5.30±2.55	[4] 96.62±115.42	[3] 10.55±13.24	[2] 8.06±4.52
KWAJALEIN	VHF (23)				
	Phase	[1] 6.24±6.72	[3] 10.15±9.34	[2] 7.15±7.65	
	Intensity	[4] 24.45±27.08	[1] 6.67±7.38	[3] 10.92±8.89	[2] 7.27±7.60
	UHF (11)				
	Phase	[1] 4.16±4.48	[3] 5.59±6.65	[2] 4.60±5.08	
	Intensity	[4] 15.58±21.07	[2] 6.75±8.31	[3] 10.35±6.44	[1] 6.46±7.25
	L-band (3)				
	Phase	[2] 1.86±1.32	[3] 1.95±1.25	[1] 1.78±1.27	
	Intensity	[2] 3.20±1.69	[4] 6.76±7.11	[3] 3.28±1.42	[1] 2.76 (single value)
POKER FLAT	VHF (12)				
	Phase	[1] 2.38±1.27	[3] 8.47±5.50	[2] 2.73±1.31	
	Intensity	[2] 20.86±22.00	[4] 149.02±159.32	[3] 29.88±56.13	[1] 8.95±8.92
	UHF (5)				
	Phase	[1] 2.38±1.42	[3] 7.16±4.19	[2] 2.43±1.43	
	Intensity	[2] 20.97±18.91	[4] 288.61±162.00	[3] 59.11±35.49	[1] 20.21±19.56
	L-band (4)				
	Phase	[2] 1.72±0.74	[1] 1.51±0.42	[3] 1.80±0.61	
	Intensity	[2] 10.03±5.79	[4] 262.97±181.09	[3] 14.75±9.14	[1?](software limit)
STANFORD	VHF (12)				
	Phase	[1] 4.49±5.21	[3] 9.18±5.70	[2] 4.91±5.72	
	Intensity	[3] 14.59±9.46	[4] 174.42±141.66	[2] 12.04±13.51	[1] 8.88±6.43
	VHF (4)				
	Phase	[1] 3.79±3.63	[3] 4.14±4.06	[2] 3.84±3.16	
	Intensity	[3] 8.49±6.01	[4] 40.35±36.43	[2] 6.81±4.24	[1] 6.66±5.13

statistics of phase are quite durable in post-scattering propagation. There is evidence, however, of measurable change in the second-order statistics -- namely, some decrease in the power-law index of the phase spectrum as intensity scintillation develops.

Regarding intensity statistics, we find no differences in ranking when changing frequency at Poker Flat or Stanford. At the two equatorial stations, where there were more cases of moderate to strong scintillation extending to higher frequencies, however, one can discern a consistent frequency trend for test results from the two classical models. That is, there is a trend for the log-normal distribution to improve its ranking and for generalized Gaussian statistics to deteriorate with increasing frequency (decreasing Fresnel-zone size). This behavior is what might be expected for transmission through a remote scattering medium having an outer-scale cutoff in its spatial spectrum, and it may be understood in terms of imposition of an effective outer scale during separation of scintillations from dispersive-phase trends.

A notable feature in Table 3 is that the relative efficacy of the two classical models is different at different stations. In particular, better intensity fits are obtained at VHF with the generalized Gaussian hypothesis than with the log-normal hypothesis for the two equatorial stations (Ancon and Kwajalein), but the reverse is true for the two higher-latitude stations. This, too, may be understood in terms of an imposed outer scale, which turns out to be geometry-dependent, as will become clear in Section III B.

A key point to be noted is that the two-component model represents an improvement over the less favored of the two classical models for every combination of frequency and observing station (eleven independent data populations) for both intensity and phase. Moreover, the two-component model provides mean χ^2 values that are nearly as favorable as (in a few instances, better than) the values for the better of the two classical hypotheses, when measured in terms of the relevant standard deviation of χ^2 or the difference in mean χ^2 between the two classical models. Thus, the two-component hypothesis provides a generally useful model for the complex-signal statistics of scintillation, including the joint pdf of intensity and phase [Eq. (23)].

The other key point is the consistency with which the Nakagami-m distribution provides a good fit to intensity data. In terms of mean χ^2, the Nakagami distribution provided the best description of intensity statistics in seven of the ten Table-3 categories for which it was reliably tested, and it was second best of the four hypotheses in the remaining three categories. The efficacy of the Nakagami-m distribution is illustrated also in Table 4, which summarizes model rankings for both phase and intensity, giving the total number of times that each model achieved each rank. Nakagami-m provided the smallest χ^2 value for intensity in 32 cases out of the 83 in which all four models were re-

liably tested, ranked second in 38 cases, was third in ten cases, and provided the least favorable fit in only three tests.

Table 4. Model Rankings
(Number of cases)

Rank		Log-normal	Generalized Gaussian	Two-Component	Nakagami-m
1	Phase	54	23	22	-
	Intensity	11	28	12	32
2	Phase	38	16	45	-
	Intensity	10	11	24	38
3	Phase	7	60	32	-
	Intensity	22	8	43	10
4	Phase	-	-	-	-
	Intensity	40	36	4	3

By comparison, the same 83 tests gave first rank to the two-component model 12 times, to the log-normal model 11 times, and to the generalized Gaussian model 28 times; the latter ranked second 11 times, third 8 times, and last 36 times. We conclude that for intensity only, Nakagami provides a more consistently good statistical distribution than either log-normal, generalized Gaussian (when the theoretical distribution is calculated from measured moments of the real and imaginary signal components), or the two-component hybrid model of Fremouw, Rino, and Livingston (1976).

Rino, Livingston, and Whitney (1976) concluded from analysis of intensity-only data that the statistics underlying complex-signal scintillation are generalized Gaussian but highly non-Rician. They obtained better fits to the generalized Gaussian model than to the log-normal model, but their method of testing the Gaussian hypothesis allowed adjustment of three free parameters, whereas the log-normal distribution was totally specified by a measured moment; therefore, their conclusion in favor of generalized Gaussian statistics was not a strong one. They did, nonetheless, use their best-fit parameters to infer that scintillation is usually accompanied by greater variance in the imaginary signal component than in the real component. The Wideband experiment has provided direct evidence in support of the latter conjecture, but it has demonstrated inadequacy of the generalized Gaussian model to provide a full description of complex-signal statistics.

The Nakagami distribution was largely ignored by Rino, Livingston, and Whitney (1976)

partly because they viewed it as virtually identical to the Rice distribution. Numerical calculations by the present authors, however, have disclosed differences between the Rice and Nakagami distributions for intermediate values of S_4 (0.4 to 0.8, say) at least as large as the differences between the log-normal and generalized Gaussian distributions compared by the former authors. Indeed, they might have found Nakagami as satisfactory as generalized Gaussian without having to vary free parameters to obtain good fits.

The shortcoming of the Nakagami model, of course, is that the m distribution has no counterpart for phase. Referring again to Table 3, we see that the log-normal hypothesis provided the smallest mean χ^2 value for phase in all 11 data categories contained in the table. Table 4 also shows that phase usually is normally distributed. Thus, a generally useful model for complex-signal statistics would be one that reduces to the product of the normal distribution for phase and the Nakagami distribution for intensity when correlation between ϕ and I is zero but that accounts, in general, for the correlation that is observed experimentally (Fremouw, Rino, and Livingston, 1976; Fremouw et al, 1978). Until such a bivariate distribution is developed and tested, the two-component model can serve to describe the full statistics of scintillating complex signals.

A final point about intensity distributions is illustrated in Figure 1, which is a plot of χ^2 values against the intensity-scintillation index, S_4, observed at Kwajalein (all frequencies). In general, the raw χ^2 values increase somewhat with increasing index, which is a measure of the spread in the histogram of observed intensity values. The significant point is that the increase in χ^2 with increasing S_4 is much more pronounced for the log-normal distribution than for the other three. This is a clear indication that the log-normal distribution, which arises from the multiplicative propagation model, is less efficacious in the "saturation" regime than are distributions arising from the additive model, which is the basis of the Nakagami and generalized Gaussian hypotheses and which plays a dominant role in development of the intensity statistics described by the two-component hypothesis. This effect may be understood in terms of a randomizing of phases in the broader angular spectrum that accompanies stronger scatter.

2. A Representative Example

Section III A 1 deals with the overall statistical behavior of approximately 100 record segments. Aside from the trends identified in that section, there is a good deal of variation from data set to data set, as is indicated by the large standard deviations of χ^2 enumerated in Table 3. In this section, we describe the behavior of a single 80-second data segment as a means of illustrating salient features in the larger data population. The segment chosen is from a pass over Ancon, starting at 0420:19 GMT on 4 March 1977 (2320:19 local civil time on 3 March) when the satellite was at an elevation of about 70° at an azimuth near 170°. The intensity scintillation index, S_4, was 0.90 (m = 1.05) at VHF,

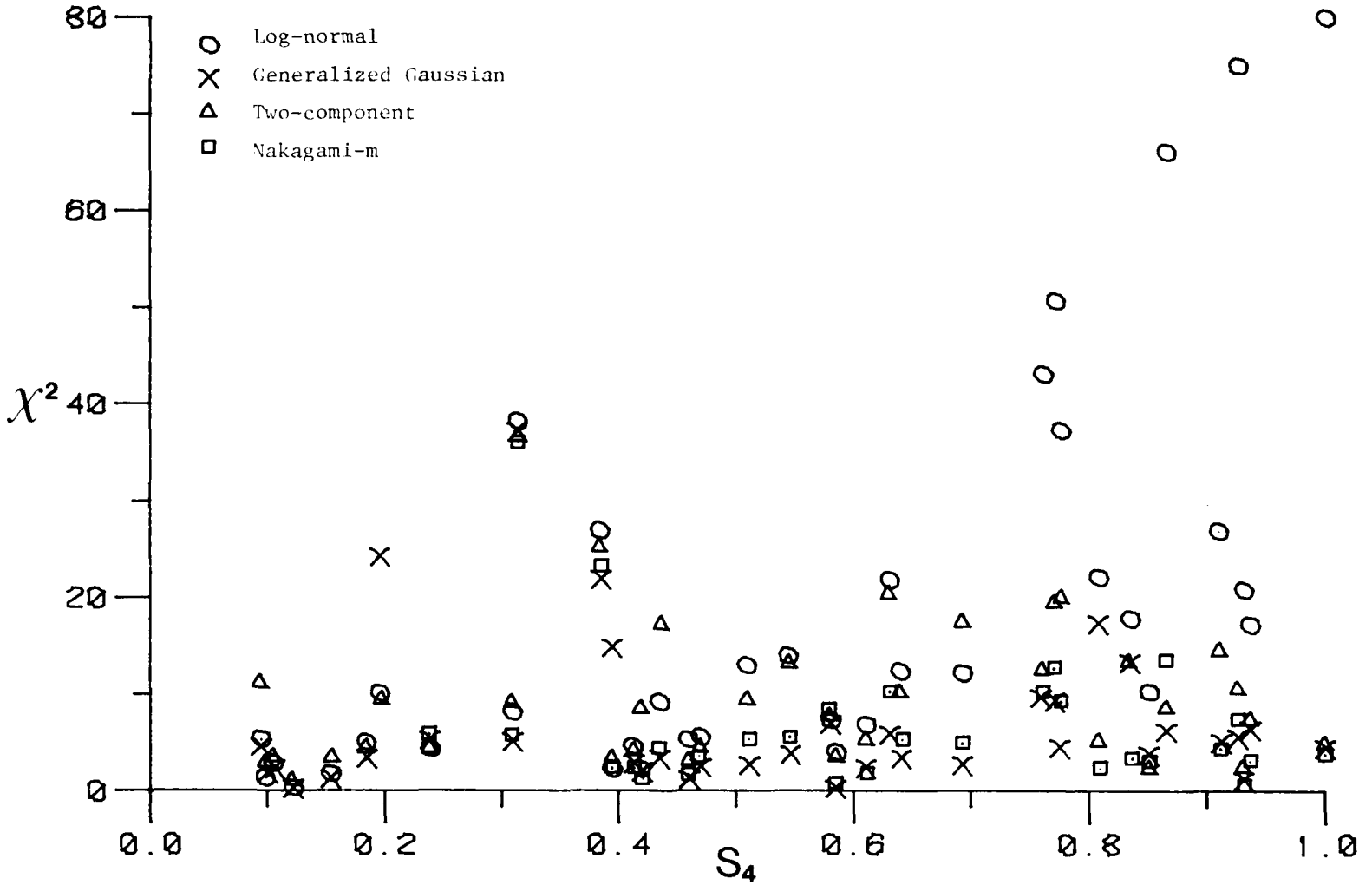

Figure 1. Relationship of goodness-of-fit parameter, χ^2, to scintillation index, S_4, for the four postulated intensity pdf's (Kwajalein, all frequencies).

0.66 (m = 1.23) at UHF, and 0.13 (m = 2.77) at L band.

Figure 2, which presents time plots of the phase, intensity, and quadrature components of the VHF signal, E, plus a scatter plot on the complex plane, suggests that the ionosphere was behaving essentially as a Rayleigh communication channel at VHF. Computed moments reveal that a little over 1% of the received power was in a steady (over ten seconds) component and that slightly over half (52%) of the fluctuation power resided in the imaginary component.

Figure 3 shows the time-series and complex-plane behavior of the two-component model's scatter component, E_s, which contained a coherent part bearing 88% of the power and a noncoherent part whose power was 56% imaginary and 44% real. The two-component model's focus component, E_f, is illustrated in Figure 4. The standard deviation, $\sigma_{\phi f}$, of the imaginary part of its complex logarithm was 2.83 radian, which accounted for most of the composite phase fluctuation, σ_ϕ = 3.32 radian, and it imposed an intensity modulation such that $\sigma_{\chi f}$ = 0.20.

The results of hypothesis testing for this case are shown in Figure 5, which displays the observed intensity and phase histograms and the theoretical pdf's calculated from the measured moments. In terms of ranking on the basis of raw χ^2 values, the behavior is typical of VHF behavior at Ancon. (Compare Table 3.) The figure illustrates well the failings of the log-normal distribution for intensity in the saturation regime: namely, that it is too peaked and underestimates the probability density for deep fades.

The generalized Gaussian hypothesis produces, for this event, essentially a Rayleigh distribution, which does not underestimate deep fades. Indeed, when p_{GI} is computed from the measured moments of x and y, it consistently overestimates deep fades. This deficiency worsens as the Fresnel-zone size decreases, as may be seen in Figure 6, which shows histogram fits for the UHF signal. The deficiency may be understood from Figure 7, which displays complex-plane scatter plots for E, E_s, and E_f at VHF, UHF, and L band. As the Fresnel radius decreases (increasing frequency), the measured value of σ_x stems decreasingly from intensity scintillations and increasingly from phase fluctuation (in relative terms). The generalized Gaussian model cannot accommodate such behavior.

Figure 8, which shows the fits for L band, demonstrates the tendency for all the pdf's to become identical for weak scatter. In the limit of very weak scatter, all the models become satisfactory; at L band in the present case, however, there is still sufficient phase fluctuation that the measured value of σ_x produces a poor generalized-Gaussian intensity fit.

The fact that good fits can be made to highly selected intensity data by optimizing free parameters in the generalized-Gaussian model, as was done by Rino, Livingston, and

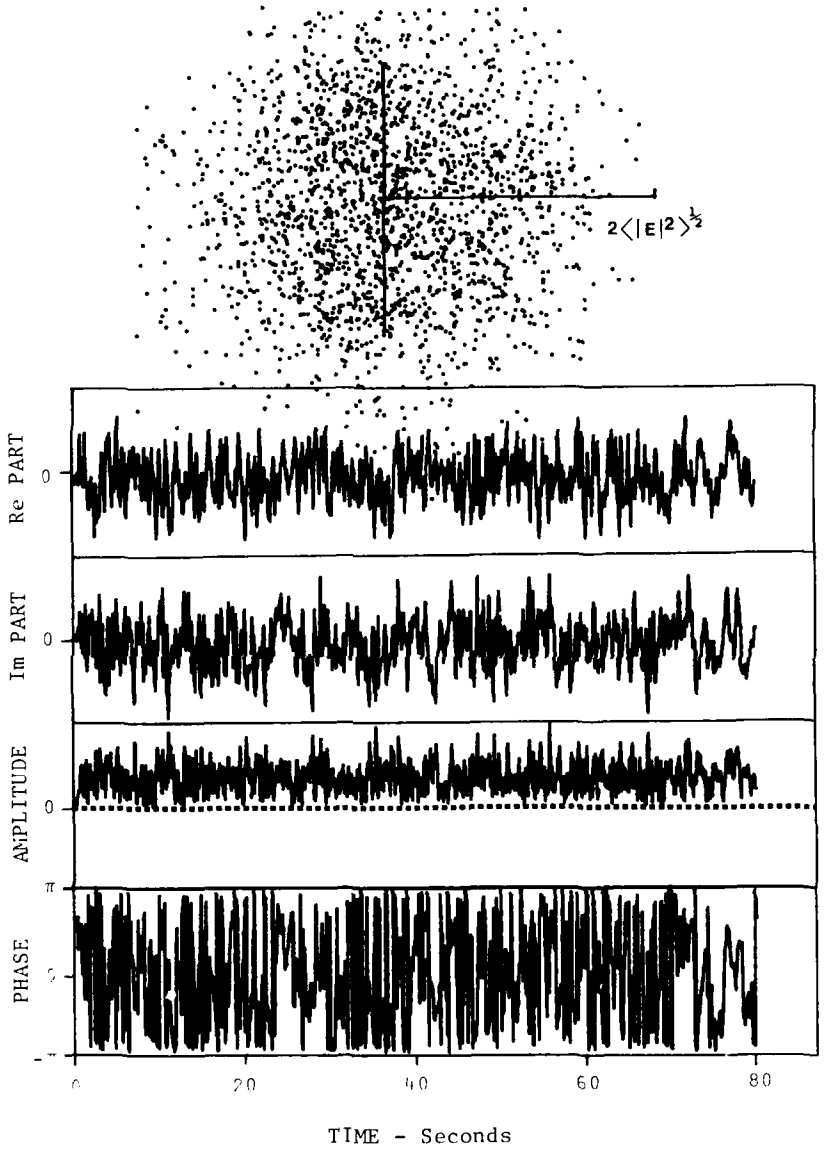

Figure 2. Three representations of complex-signal scintillations observed at 138 MHz at Kwajalein, starting at 0420:19 GMT on 4 March 1977. Top to bottom: scatter plot on the complex plane; real and imaginary parts of the complex signal; amplitude and phase of the complex signal.

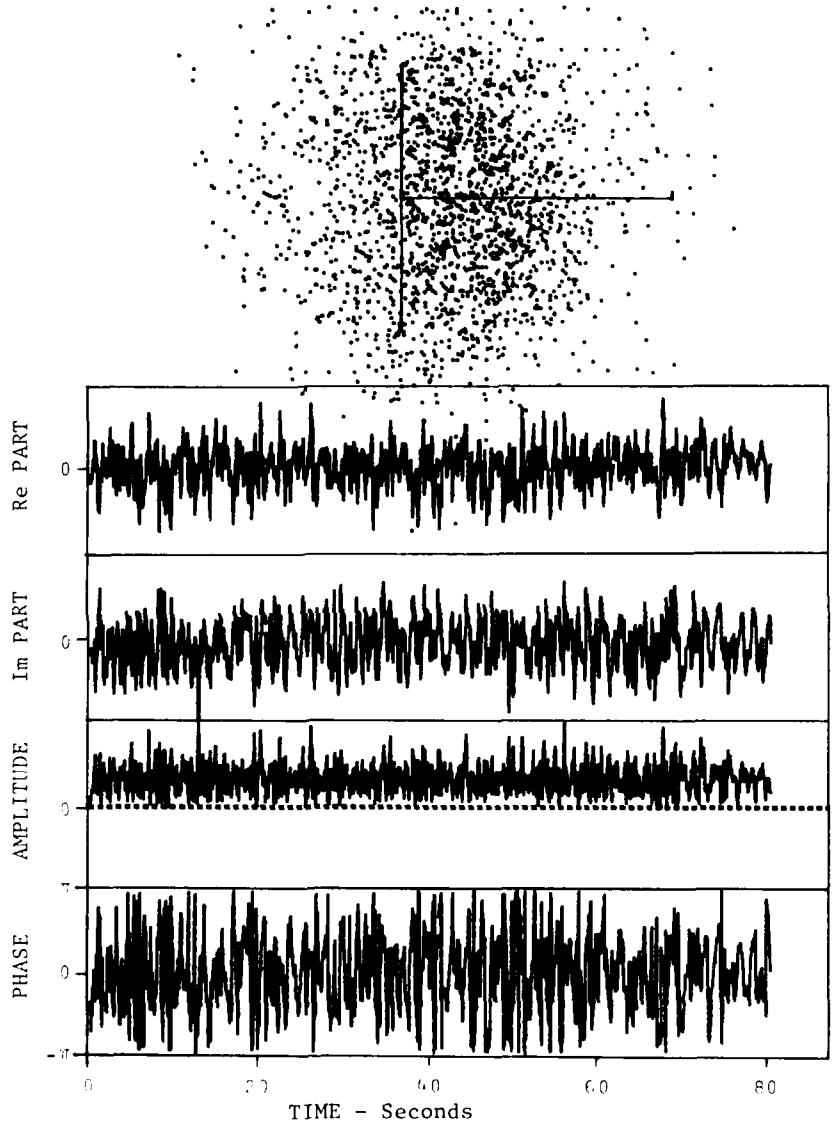

Figure 3. The "scatter" component, E_S. of the signal shown in Figure 2, containing phase and log-amplitude fluctuations with Fourier periods shorter than 2.5 seconds (isolated by means of "dual detrending").

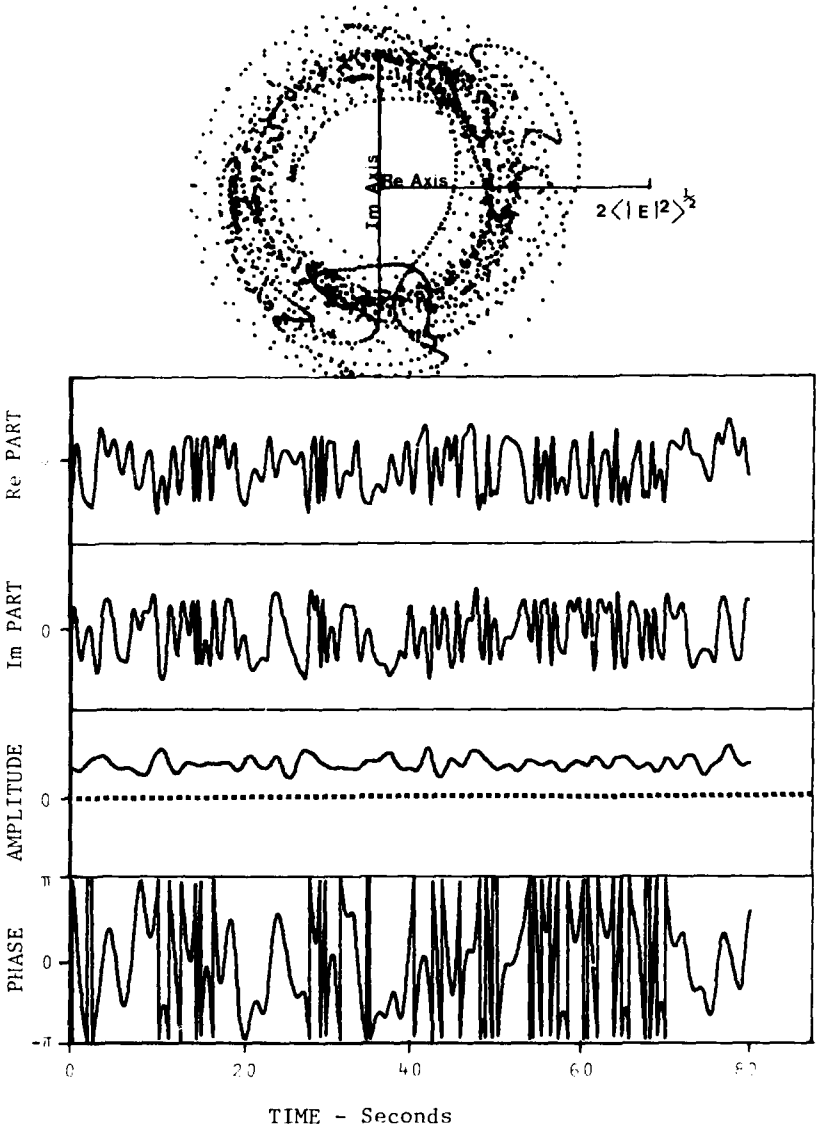

Figure 4. The "focus" component, E_f, of the signal shown in Figure 2, containing phase and log-amplitude fluctuations with Fourier periods between 2.5 and ten seconds (isolated by means of a ten-pole, low-pass Butterworth filter).

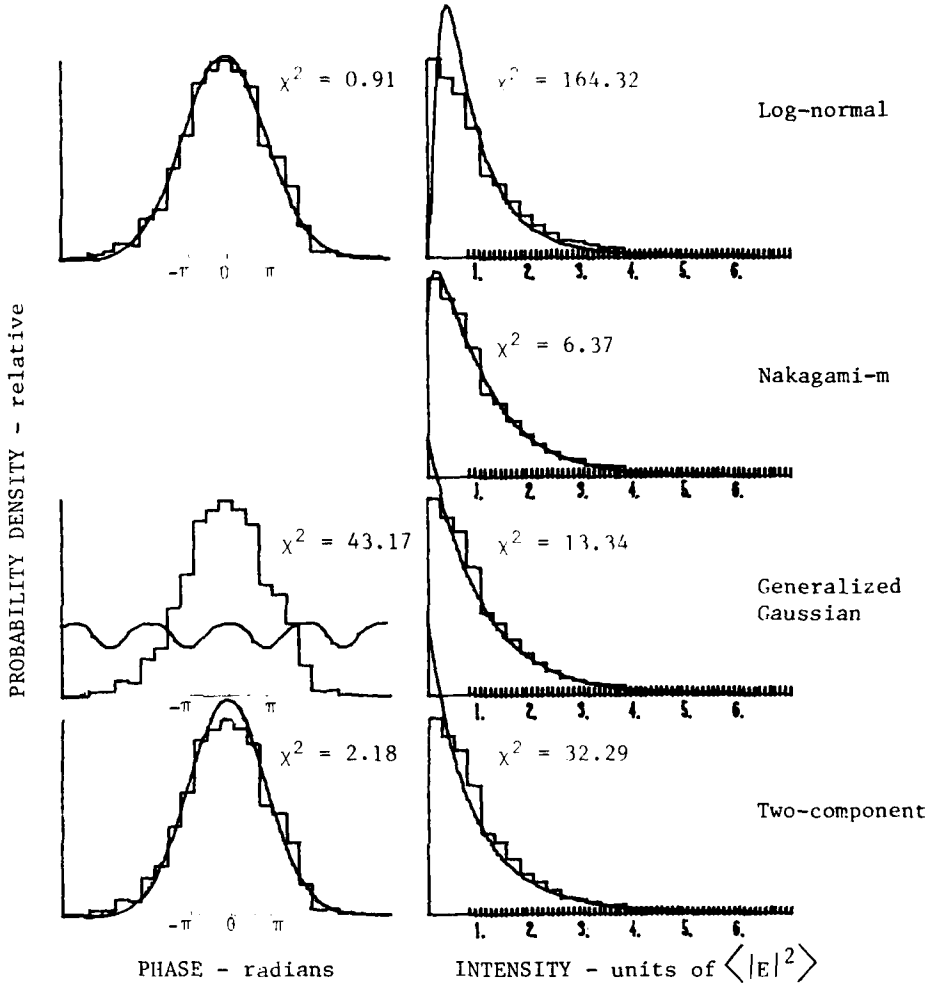

Figure 5. Histograms of phase and intensity of the VHF signal shown in Figure 2, compared with probability density functions (pdf's) calculated on the basis of four signal-statistical hypotheses.

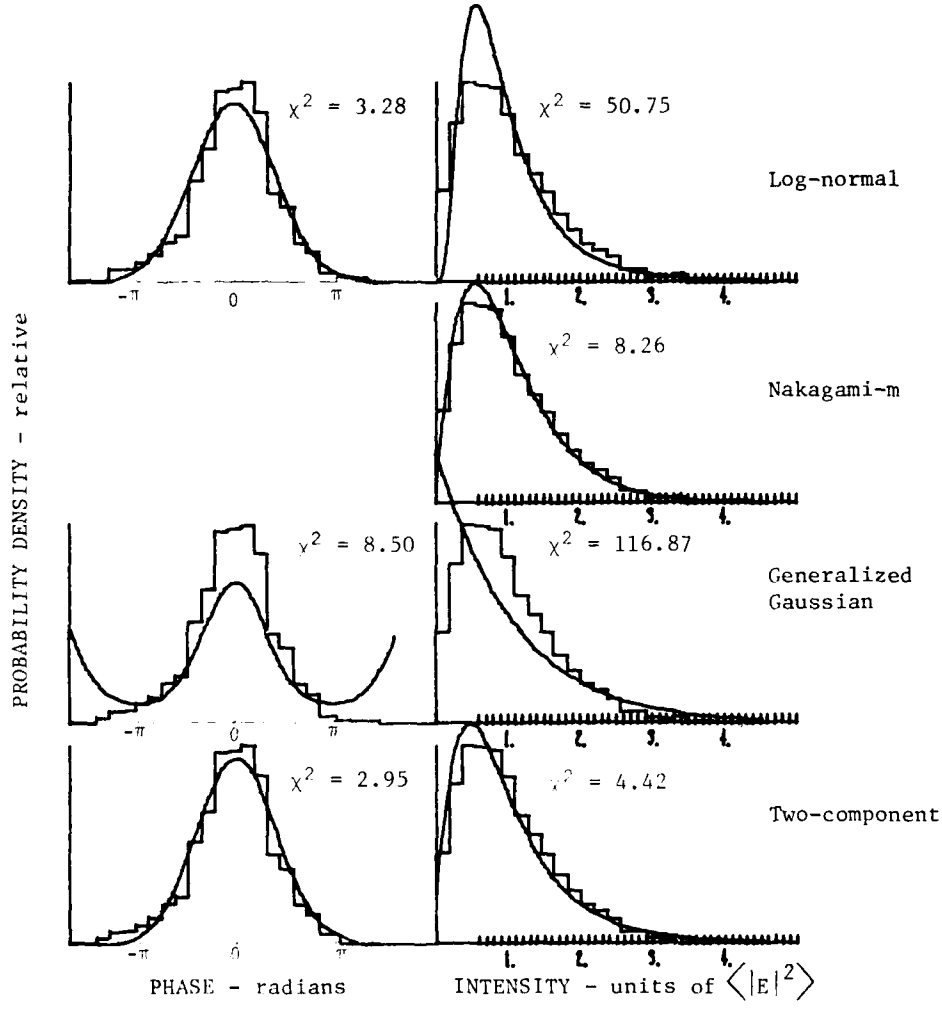

Figure 6. Histograms of phase and intensity of the UHF (379-MHz) signal received simultaneously with the VHF signal shown in Figure 2, compared with calculated pdf's.

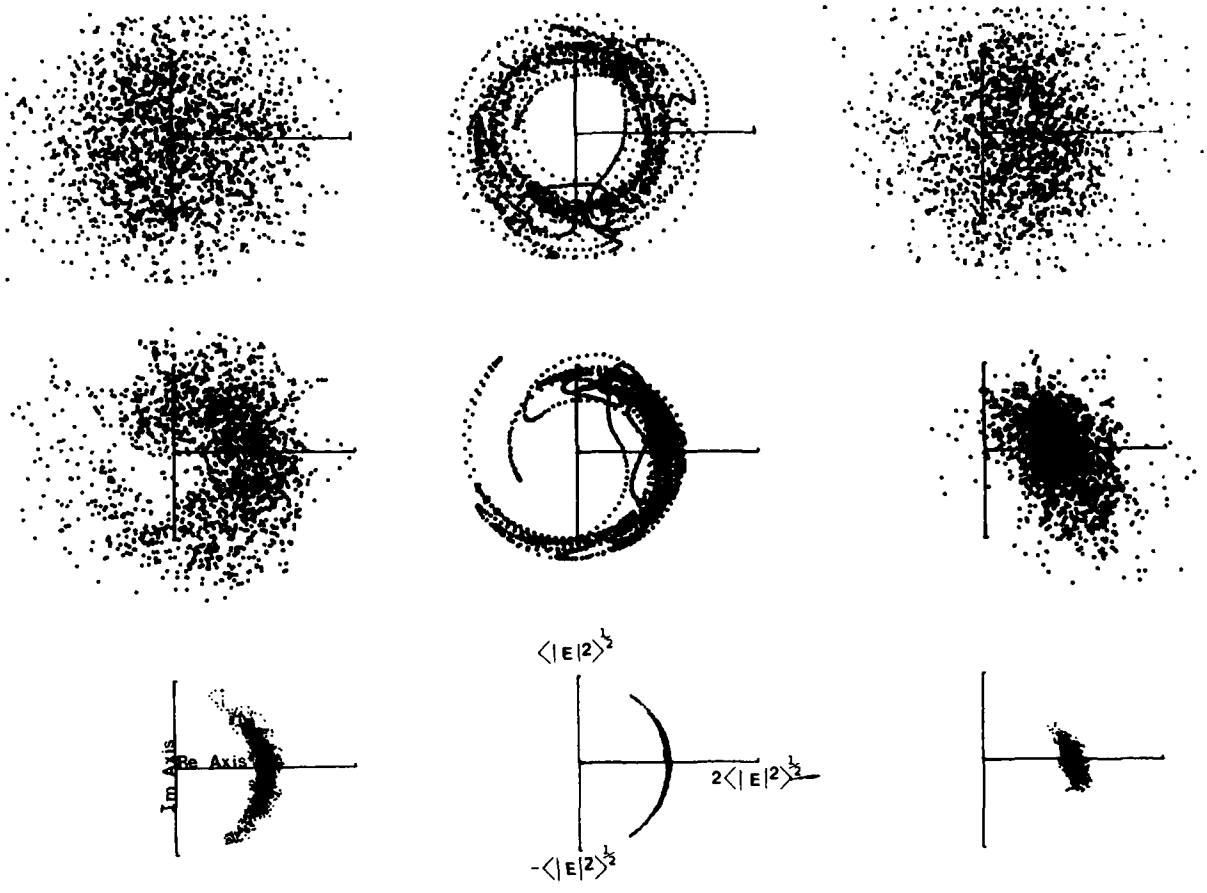

Figure 7. Complex-plane scatter plots for the VHF (top), UHF (middle), and L-Band (bottom) signals received at Kwajalein during the 80 seconds beginning at 0420:19 GMT on 4 March 1977. Left: composite signal, E. Center: focus component, E_f. Right: scatter component, E_s.

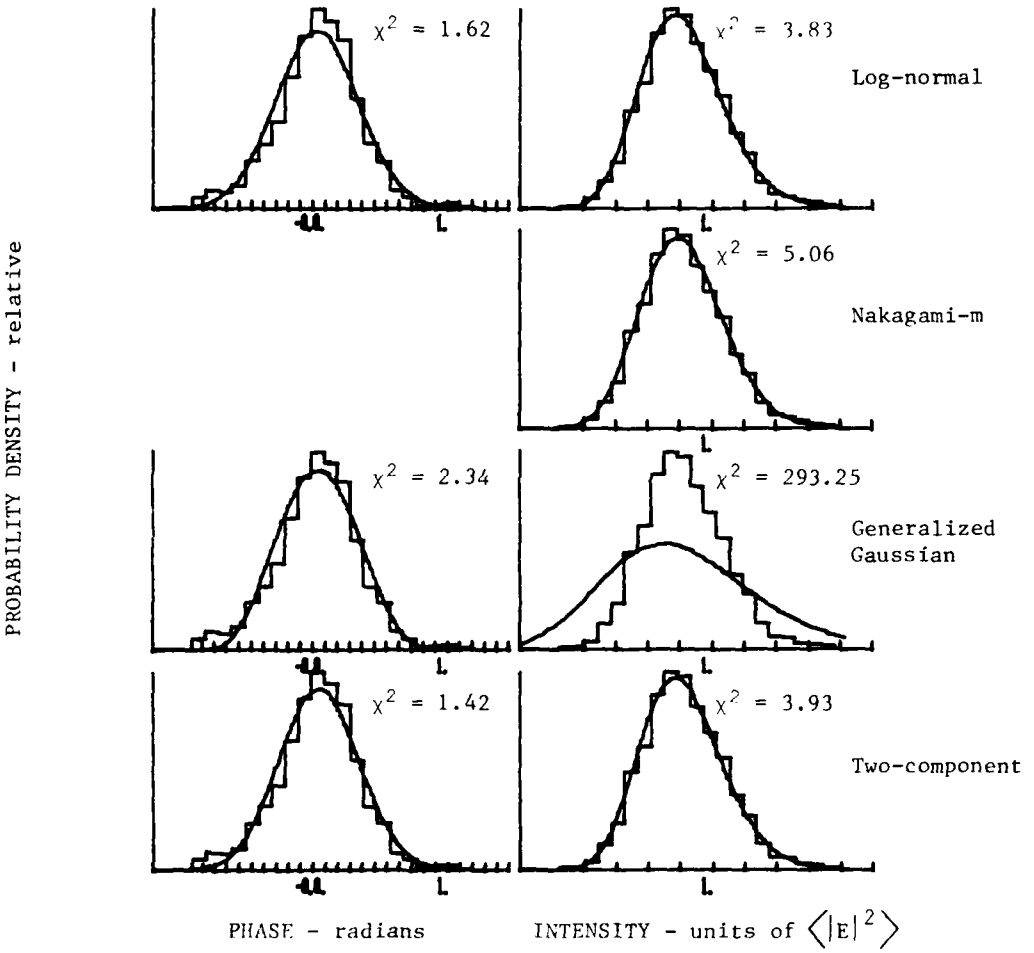

Figure 8. Histograms of phase and intensity of the L-Band (1239-MHz) signal shown at the bottom of Figure 7 and received simultaneously with the VHF signal shown in Figure 2 (and at the top of Figure 7), compared with calculated pdf's.

Whitney (1976) suggests that a component of complex-signal scintillation might obey such statistics. This conjecture formed part of the experimental basis for the two-component hypothesis of Fremouw, Rino, and Livingston (1976).

Figure 5 illustrates the fact that, when the intensity distribution approximates p_{GI}, the two-component model retains the essential characteristics of generalized-Gaussian statistics as they pertain to intensity, providing a fit that is better than p_{ℓ} and nearly as good as p_{GI}. Figures 6 and 8 illustrate the durability of the two-component model as the Fresnel-zone radius decreases toward a regime where log-normal statistics are satisfactory.

Figure 9 compares histograms of x_s and y_s and of χ_f and ϕ_f, for L band, with normal distributions. Its top two plots, together with the complex-plane scatter diagram for E_s at L band in Figure 7, reveal a truly generalized-Gaussian component. It is because this component usually dominates intensity scintillations that Rino, Livingston, and Whitney (1976) were able to obtain good intensity fits on the basis of the generalized-Gaussian hypothesis. Isolation of an accurately Gaussian component, however, requires a good deal of data manipulation and sets aside another component of complex-signal scintillation.

Figure 5 also illustrates (with, in fact, unusual fidelity) the consistent result that phase scintillations are well described by a normal distribution. It demonstrates, further, that the two-component model retains this essential behavior, yielding a phase pdf only slightly less efficacious than the log-normal model and far better than the generalized-Gaussian hypothesis. In contrast, the generalized-Gaussian model provides no mechanism for describing phase beyond a modulo-2π definition.

A strictly formal test of the phase pdf arising from the generalized-Gaussian hypothesis would be to compare the pdf with a histogram of phase values for which 2π ambiguities have not been resolved. To do so in the present work, however, would have been to treat the data differently for different hypotheses; it was decided, instead, to treat the data identically in every case and to accept poor phase fits as a quantitative statement of the qualitatively obvious limitation of generalized-Gaussian statistics in the presence of large phase excursions.

In performing the tests, it was supposed that the phase pdf repeated itself in every 2π range for which phase values were observed. Normalization was carried out to match the area under the pdf with that under the observed histogram over the range of bins containing values. An alternative would have been to match the area under the pdf in the range $-\pi$ to $+\pi$ with that under the entire histogram, which also would have produced large χ^2 mismatches.

A further point demonstrated in Figure 5, et sequel, is the efficacy of the Nakagami-m distribution in describing intensity scintillation. As was discussed in Section III A 1 and illustrated in Tables 3 and 4, this was one of the most consistent results of hypoth-

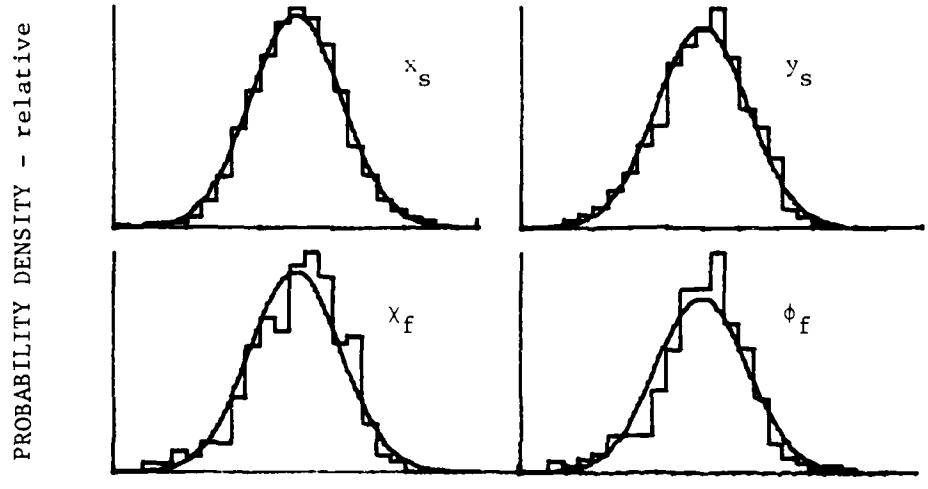

Figure 9. Histograms of the real (left) and imaginary (right) parts of the scatter component (top) and the logarithm of the focus component (bottom) of the L-band signal shown at the bottom of Figure 7, compared with normal pdf's computed from the measured means and variances.

esis testing. Figure 5 points up particularly well that a bivariate distribution reducing to the product of the Nakagami-m distribution for intensity and the normal distribution for phase in cases of no correlation between the variates, would provide a suitable model for complex-signal scintillation.

Figure 7, however, illustrates the fact (particularly at UHF) that such correlation is a salient feature of scintillating signals. It may well be unimportant in many applications, but it cannot be ignored in a general statistical description of scintillation. Furthermore, it can be calculated as a function of Fresnel distance (Fremouw and Rino, 1978). That the two-component hypothesis, which does account for correlation, provides an efficacious model, also is illustrated in Figure 5, et sequel. The two-component model also provides some intuitive basis for understanding signal-statistical behavior, although at the expense of requiring six parameters (the "six sigmas") for its specification.

We have dealt only with raw χ^2 values for assessing efficacy of the four models. In general, the raw χ^2 values are consistent with the impressions one gains from inspection of graphical histogram fits. For hypothesis testing in the strict sense, one would want to establish levels of confidence, which can be done for individual data sets but not for the mean χ^2 values appearing in Table 3.

Even for individual data sets, subtle questions arise regarding the number of degrees of freedom lost in computing the intensity and phase pdf's on the basis of complex-signal moments (for the generalized Gaussian and, particularly, the two-component hypotheses). Suffice it to say that a wide range of confidence levels (from 0.01% to 99.5%) has been calculated on the basis of reasonable assumptions about degrees of freedom lost and that the rankings of the various hypotheses have remained the same as those established by means of the raw χ^2 values.

B. GEOMETRICAL CONTROL OF THE RATIO, S_4/σ_ϕ

1. Relevant Theoretical Expressions

In Section III A, we explored the variation of complex-signal statistics with observing frequency, scattering strength, and receiver location but postponed a detailed description of geometrical factors. The purpose of this section is to provide such a description, not in terms of the statistical distributions but in terms of the two most relevant moments that control them: namely, the phase and intensity scintillation indices, σ_ϕ and S_4 $(=m^{-\frac{1}{2}})$. One of the first features of complex-signal statistics noted in Wideband data was a sizeable difference in the ratio of S_4 to σ_ϕ when measured at Stanford, Poker Flat, and Ancon (Fremouw and Livingston, 1976). Later it was found that both equatorial stations, Ancon and Kwajalein, consistently show a higher S_4/σ_ϕ ratio than does Poker Flat, for nonsaturated intensity-scintillation conditions (Fremouw, 1978a).

Rino has developed weak-scatter expressions, based on the phase-screen propagation model, that are suitable for interpreting both phase (Rino and Fremouw, 1977) and intensity (Rino and Matthews, 1978) scintillation records in terms of a fairly general description of irregular plasma structure. We employ here his expressions for σ_ϕ and S_4, finding that the observed differences in their ratio may be explained in terms of scattering-geometry control in the presence of an outer scale that falls outside our data window. We suggest that the same effect causes the latitudinal and Fresnel-zone-size dependences of best-fit, signal-statistical models noted in Table 3.

Recalling that the detrending procedure employed in Wideband data processing behaves like a sharp-cutoff, high-pass filter (Fremouw, 1978b), we may write the square of the phase scintillation index succinctly as

$$\sigma_\phi^2 = \frac{2T\, f_o^{(1-2\nu)}}{2\nu-1} \tag{26}$$

where T = power-spectral density of phase at 1 Hz,

f_o = detrender cutoff frequency,

and ν = power-law spectral index describing the spatial spectrum of scattering irregularities (obtained with resonable accuracy as half the measured index of the phase power spectrum).

Rino's formulation relates the measured strength of the phase spectrum to ionospheric and geometrical parameters as

$$T = (r_e^2 \lambda^2 L \sec\theta)\, G\, C_s \left[\frac{\sqrt{\pi}\,\Gamma(\nu)}{(2\pi)^{2\nu+1}\Gamma(\nu+\frac{1}{2})} \right] V_e^{2\nu-1} \tag{27}$$

where r_e = classical electron radius,

λ = radio wavelength,

and θ = incidence angle.

The gamma functions arise from normalizing the three-dimensional ionospheric spectrum to $\left\langle (\Delta N)^2 \right\rangle$, and the main geometrical factor is

$$G = \frac{a\, b}{\sqrt{AC - B^2/4}\,\cos\theta} \tag{28}$$

where a and b are irregularity axial ratios along and across the geomagnetic field, respectively, and A, B, and C are geometrical parameters given in Eq. (41) of Rino and Fremouw (1977). The strength of the scattering structure is described as

$$C_s = 8\pi^{3/2} \frac{\Gamma(\nu+\frac{1}{2})}{\Gamma(\nu-1)} q_o^{2\nu-2} \langle \Delta N^2 \rangle \tag{29}$$

which is (to within a factor ab, which Rino chose to incorporate in G) numerically equal to the strength of the "isotropized" three-dimensional spectrum at a wave number of 1 radian/m. The spectrum is supposed to be cut off at a very large outer scale, q_o^{-1}.

The remaining quantity in Eq. (27) is the "effective velocity", V_e, which is the speed with which the radio line of sight cuts across contours of equal correlation in the ionosphere (or alternatively with which contours of phase correlation scan across the receiver). The effective velocity accounts for the effect that anisotropy of the irregularities has on the conversion of spatial structure to temporal fluctuations; it is related to scan velocity in isotropic coordinates by means of Eq. (12) of Rino and Matthews (1978).

The square of the intensity scintillation index developed in Rino and Matthews (1978) is

$$S_4^2 = 4(r_e^2\lambda^2 \, L \sec\theta) \, F \, C_s \left\{ \frac{-\Gamma(\frac{1-2\nu}{2})\cos\left[\pi(1-2\nu)/4\right]}{2\pi \, 2^{(5-2\nu)/2}} \right\} Z^{\nu-\frac{1}{2}} \tag{30}$$

in which diffraction is described primarily by the Fresnel-zone parameter

$$Z = \frac{\lambda z \sec\theta}{4\pi} \tag{31}$$

where z is the effective "reduced height" (including correction for wavefront curvature) of the irregularities. The major theoretical result presented in Rino and Matthews (1978) is evaluation of the geometry-dependent Fresnel filter factor, F, as

$$F = \frac{ab}{\sqrt{A''} \, C''^{\nu}} \, {}_2F_1\left(\tfrac{1}{2}-\nu, \tfrac{1}{2}; 1; \frac{A''-C''}{A''} \right) \tag{32}$$

where A" and C" are geometrical parameters derived from A, B, and C by means of a coordinate rotation and where ${}_2F_1$ is the Gaussian hypergeometric function. Rino and Matthews (1978) combined Eqs. (27) and (30) into the following succinct description of the dependence of the intensity scintillation index on the strength of the phase perturbation produced by the ionosphere:

$$S_4^2 = 4C(\nu) \frac{T}{V_e^{(2\nu-1)}} \frac{F}{G} Z^{\nu-\frac{1}{2}} \tag{33}$$

The dependence of intensity scintillation on the shape of the ionospheric-irregularity

power spectrum is a bit complicated, with the spectral index appearing in Eq. (33) in four different factors, including

$$C(\nu) = \frac{-(2\pi)^{2\nu}\Gamma(\frac{1}{2}-\nu)\Gamma(\frac{1}{2}+\nu)\cos\left[\frac{\pi(1-2\nu)}{4}\right]}{\sqrt{\pi}\,\Gamma(\nu)\,2^{(5-2\nu)/2}} \tag{34}$$

For a one-dimensional irregularity spectrum of k^{-2}, as is often observed in situ (Dyson, McClure, and Hanson, 1974), $\nu = 1.5$. Unfortunately, Eq. (34) takes on the indeterminate value 0/0 in this case [as does the factor in curly brackets in Eq. (30)].

However, by applying recurrence and reflection formulas for the gamma function (Abramowitz and Stegun, 1964) and a trigonometric identity, one may show that Eq. (34) is equivalent to

$$C(\nu) = \frac{-\sqrt{\pi}(2\pi)^{2\nu}(\cos\frac{\pi}{4}\cos\frac{\pi\nu}{2} + \sin\frac{\pi}{4}\sin\frac{\pi\nu}{2})}{2^{(5-2\nu)/2}\Gamma(\nu)\cos(\pi\nu)} \tag{35}$$

which, by means of some additional trigonometric relations, may be simplified to

$$C(\nu) = \frac{2^{3\nu}\pi^{2\nu}}{-4\sqrt{2/\pi}}\,\frac{\cos\left[\pi(\frac{\nu}{2}-\frac{1}{4})\right]}{\Gamma(\nu)\cos(\pi\nu)} \tag{36}$$

A single application of L'Hopital's rule then shows that

$$\lim_{\nu\to 1.5} C(\nu) = 4\pi^3 \tag{37}$$

Figure 10 is a plot of Eq. (36) and (37), showing that $C(\nu)$ mitigates somewhat the tendency for S_4 to increase with decreasing spectral index via the Fresnel filter factor, F, and the factor $V_e^{1-2\nu}$ in Eq. (33), as does the factor $Z^{\nu-\frac{1}{2}}$.

2. Application to Investigation of the Scintillation-Index Ratio

Eq. (33) gives the intensity-scintillation index in terms of the phase power-spectral density, T. To obtain the intensity variance per unit phase variance experienced by a system with a high-pass cutoff, f_o, we divide Eq. (33) by Eq. (26) to obtain

$$\frac{S_4^2}{\sigma_\phi^2} = [2(2\nu-1)C(\nu)]\left(\frac{f_o}{V_e}\right)^{2\nu-1}\frac{F}{G}\,Z^{\nu-\frac{1}{2}} \tag{38}$$

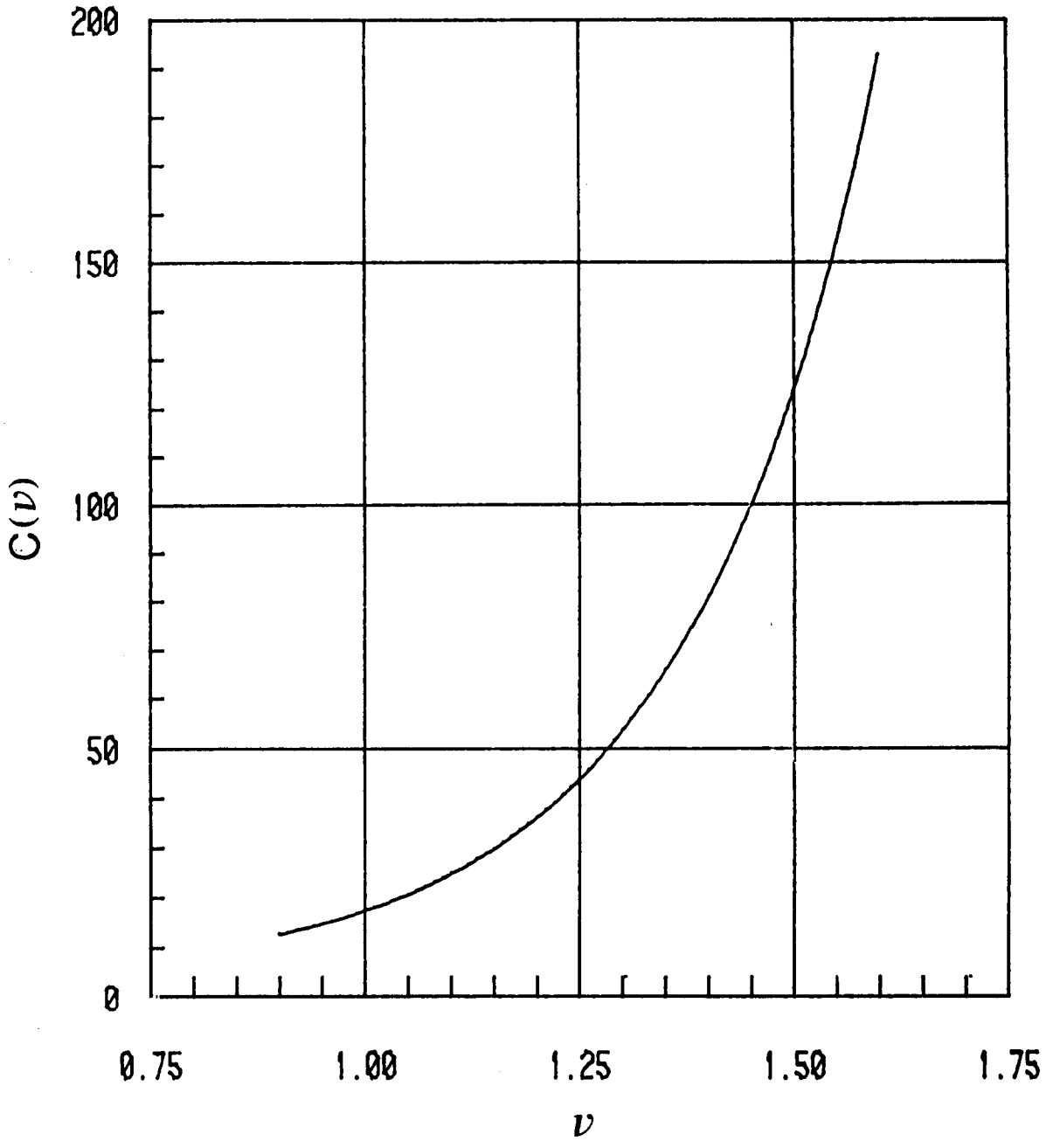

Figure 10. The factor C(ν), which tends to mitigate the increase of S_4 with decreasing spectral index, ν, due to other factors in Eq. (30).

Various observers have reported differences in the spectral index, p, inferred from scintillation measurements made at different locations (Whitney and Basu, 1977; Rino et al, 1978; Rino and Matthews, 1978), which could produce differences in the scintillation-index ratio. To the extent that the spectral index displays a systematic latitude dependence, however, it appears to be in the sense of smaller values of p in auroral than in equatorial regions. This is opposite the sense required to explain the observed S_4/σ_ϕ behavior under study here.

The other obvious candidate for explaining the observed behavior is the possibility of different effective heights for the relevant striations at different latitudes, which would affect Eq. (38) directly through Z. Rino and Matthews (1978) have pointed out, however, that this dependence is complicated by the indirect effect of irregularity height on V_e (by way of the scan velocity for a given satellite).

In the work reported in this section, we held p and the irregularity height constant in order to investigate the role that factors having to do with striation shape and experiment geometry might play in establishing the S_4/σ_ϕ ratio. We then performed comparative calculations for VHF data sets from two Wideband passes - Poker Flat Pass 6-39, observed on 28 July 1976, and Kwajalein Pass 22-13, observed on 28 October 1977. Figure 11 illustrates the reason for selecting these two samples, which contain 60 seconds of data from near 1020 GMT (0020 local time) and 85 seconds of data from near 1228 GMT (0028 local time), respectively.

The figure shows plots of S_4 versus σ_ϕ for VHF data sets from all four Wideband stations for which dual-detrend analysis has been carried out. The data sets were carefully selected to include a wide range of observing geometries and scintillation levels and to provide reasonable statistical stationarity. The two data sets marked on the figure were chosen for this investigation of S_4/σ_ϕ because they are representative of results at an equatorial and an auroral-zone station under conditions of essentially identical, moderate intensity scintillation.

To investigate the clear-cut difference between behavior at Poker Flat and at the two equatorial stations, the known observing geometry associated with the two data points identified in Figure 11 was employed, along with several irregularity models, to calculate various factors appearing in Eq. (38). Finally, the factors were combined to calculate the scintillation-index ratio itself, the results of which are shown in Figure 12.

The first model employed was that of axially symmetric striations aligned along the geomagnetic field. For this model, the single axial ratio was stepped from unity (isotropic irregularities) to 40:1, as shown on the steep solid curve in the figure. Values of S_4/σ_ϕ were calculated from the model and from the known ionospheric incidence angle and geomagnetic

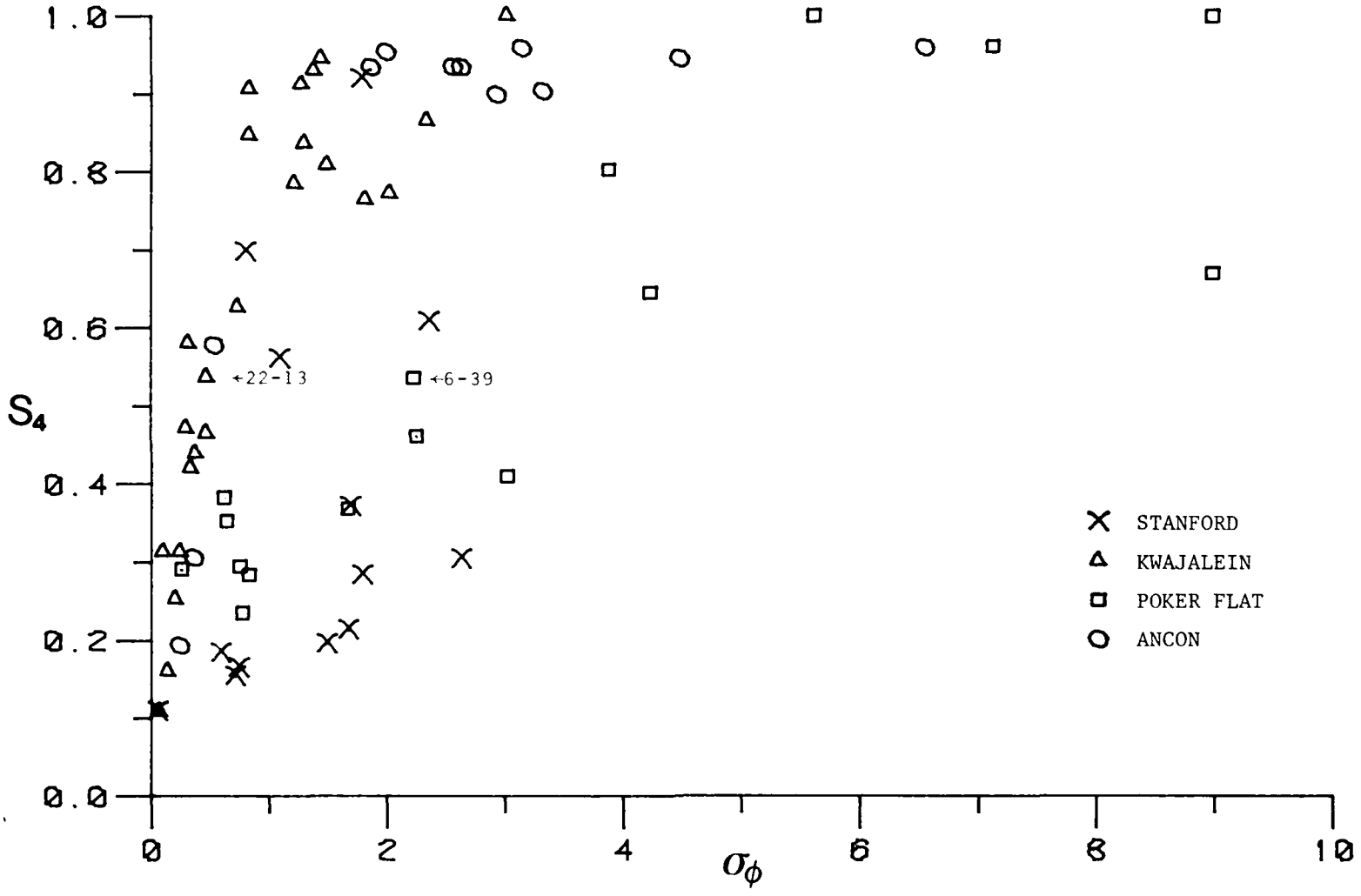

Figure 11. Scatter diagram of scintillation indices for intensity (S_4) and phase (σ_ϕ) for 62 VHF data segments ranging in length from 20 to 85 seconds. Note consistency of pattern from two equatorial stations, Kwajalein and Ancon, and separate pattern formed by data from a high-latitude station, Poker Flat.

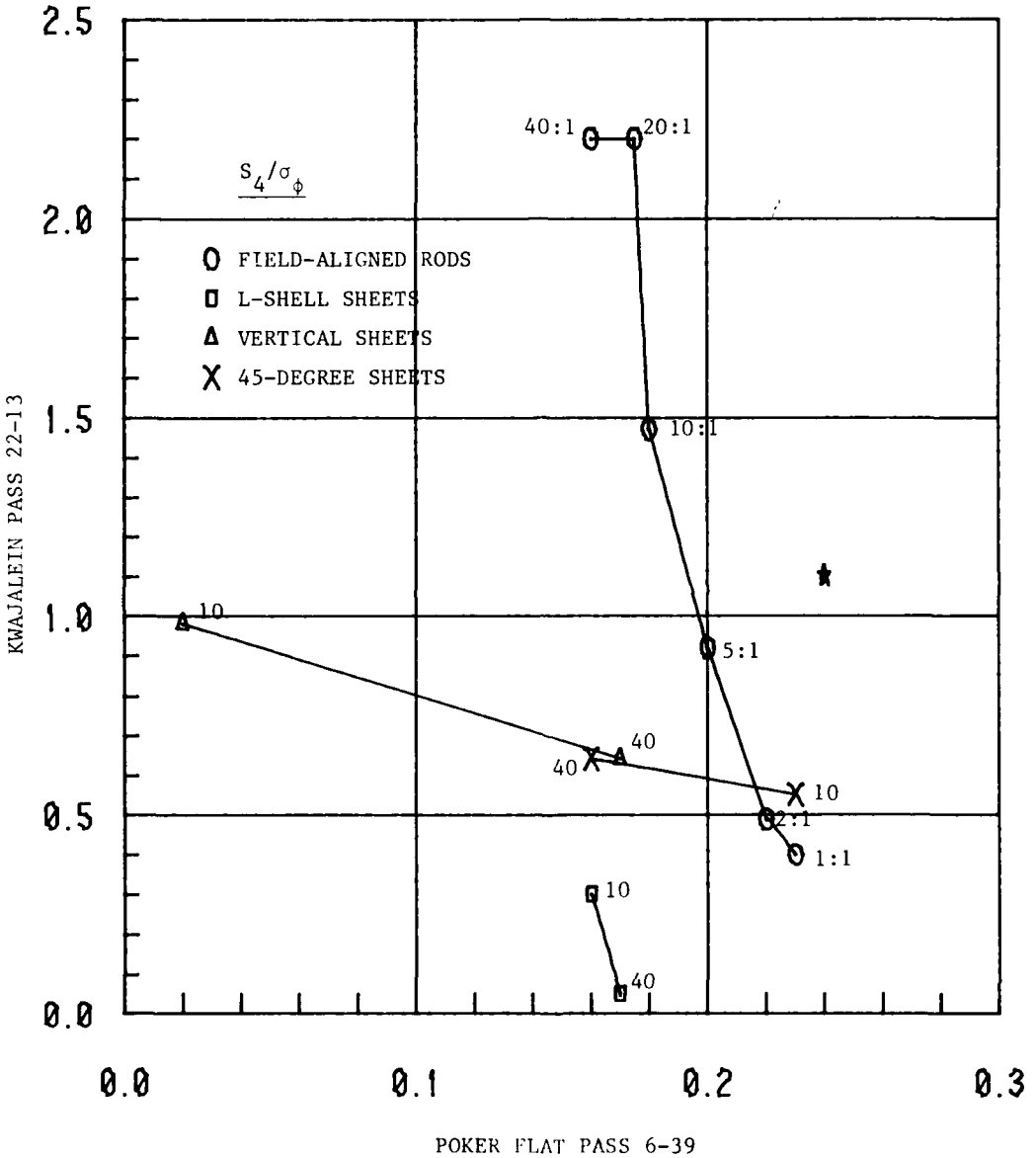

Figure 12. The ratio of intensity scintillation index, S_4, to phase scintillation index, σ_ϕ, for a 60-second data set from Poker Flat (horizontal axis) and an 85-second data set from Kwajalein (vertical axis). Isolated point at (0.24, 1.10) represents observed data. Other points are calculated from various rod and sheet irregularity models. Numbers by points are axial ratios. (All sheet models have two-dimensional isotropy; that is, 10 means 10:10:1 and 40 means 40:40:1.)

heading of the propagation vector and scan velocity of the line of sight, for each of the two data sets. The results for the two samples were then plotted on a common grid, as were the observed scintillation-index ratios (isolated point at 0.24, 1.10).

Next, sheet-like irregularity models were invoked and the calculations repeated. Three such models were employed: sheets layered like onion skins along L shells, such as have been observed from Poker Flat (Fremouw et al, 1977) and possibly at a middle latitude in the southern hemisphere (Hajkowicz, 1978); vertical sheets lying in the magnetic meridian plane; and sheets oriented at 45° to both the meridian plane and the L shells, tilted from upper west to lower east as some backscatter plumes appear to be (Fremouw and Lansinger, 1977; Tsunoda, Baron, and Owen, 1978). For each sheet model, the calculation was performed for axial ratios of 10:10:1 and 40:40:1.

The first point to be noted from Figure 12 is that all models but one (40:40:1 sheets aligned on L shells) produced a greater S_4/σ_ϕ ratio for Kwajalein than for Poker Flat. Thus, one is led immediately to suspect that something inherent in the geometry produces the observed difference. It happens that the ionospheric incidence angle, θ, is larger for the Kwajalein data set (54.5°) than for the set from Poker Flat (17.9°). This fact alone is sufficient to produce a slightly greater scintillation-index ratio in the K22-13 data set than in the PF6-39 set, as seen in the point calculated for isotropic irregularities (1:1 rods). It is not sufficient, however, to reproduce the observed data point. Indeed, only five of the 12 models employed produced calculated points lying on or above a line between the origin of Figure 11 and the observed data point.

There is no reason to suppose *a priori* that the same irregularity model is appropriate at both Kwajalein and Poker Flat. As an aside, it is interesting to note that few of the models invoked produce enough diffraction to yield S_4/σ_ϕ ratios as large as those observed at either station (for the assumed values of ν and irregularity height), although several come close at Poker Flat. Highly elongated rod-like striations, however, have no difficulty producing the large S_4/σ_ϕ ratio observed at Kwajalein.

The main thrust of this analysis is to attempt to isolate the factor that dictates the large disparity in scintillation-index ratio observed at the two stations. The final two figures present a comparison between two relevant factors. Figure 13 shows calculated results for the ratio of the Fresnel-diffraction filter factor, F, to the phase-scintillation geometric enhancement factor, G. This ratio contains most of the "static" effect of diffraction. That is, it is independent of source motion and therefore of temporal filtering operations such as detrending.

The key point to note in Figure 13 is that all models produce calculated points lying on (isotropic only) or below (all other models) a 45° radial from the origin of the calcu-

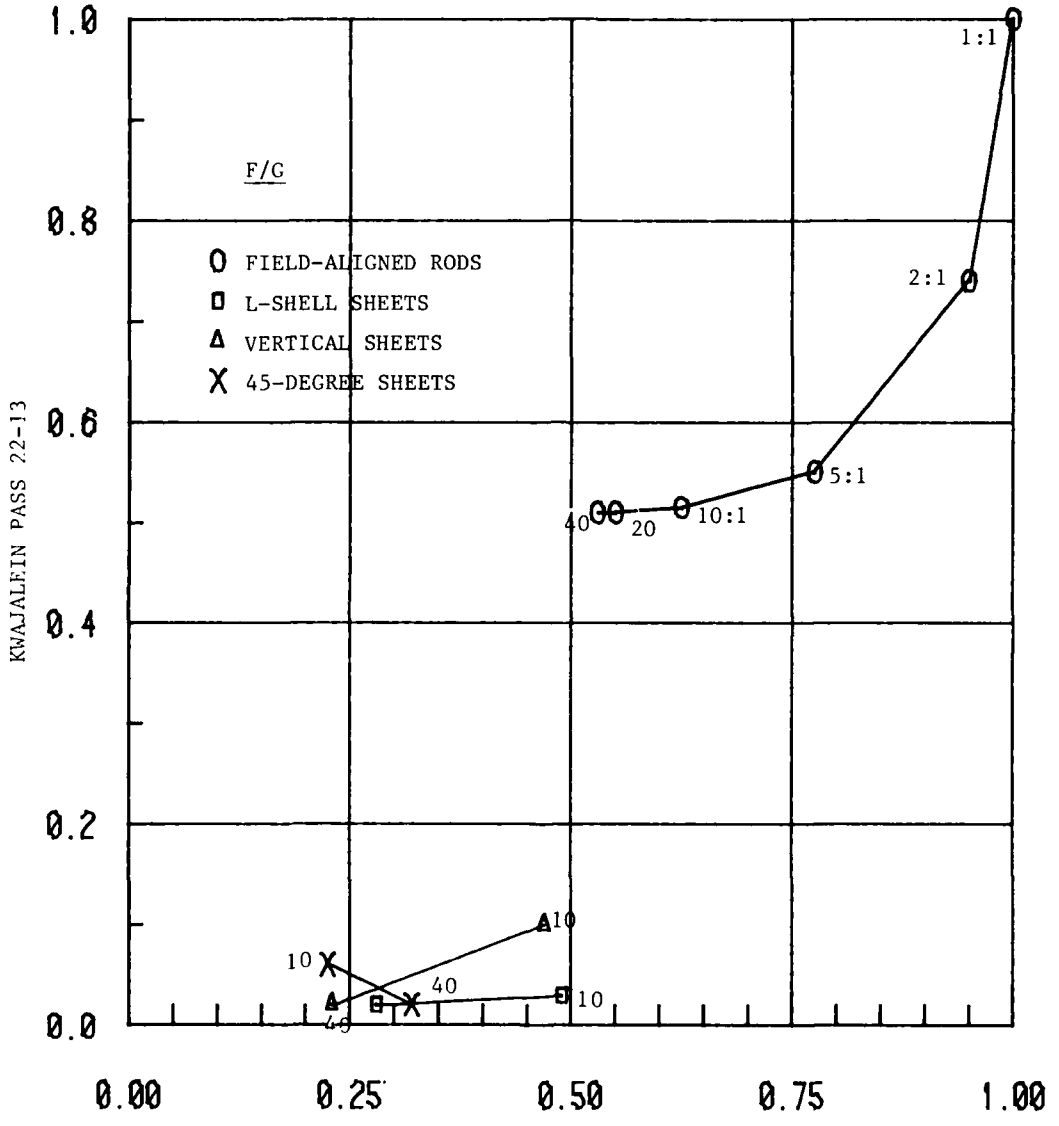

Figure 13. Calculated values of the main geometrical factor controlling "static" diffraction: i.e., the ratio of the Fresnel-diffraction filter factor, F, to the phase-scintillation enhancement factor, G.

lation grid. That is, all of the models invoked produced more diffraction at Poker Flat than at Kwajalein (aside from sec θ factors that are not included in F and G). While not anticipated, this fact probably results from the element of alignment along the geomagnetic field (which is horizontal at Kwajalein and highly inclined at Poker Flat) that is inherent in all the models. The main point is that effects of static geometry are in the opposite sense from that needed to explain the observed disparity in scintillation-index ratio.

The situation reverses abruptly when one considers source motion and the effect of detrending on phase scintillation, as demonstrated in Figure 14. The ratio f_o/V_e is the spatial-filter cutoff (in units of m^{-1}) imposed by the detrender on the isotropically expressed nonisotropic spatial spectrum of phase fluctuations. In effect, it translates the detrend filter not only from time to space but also from the actual scan direction to an euqivalent scan across the narrow dimension of the scattering irregularities (i.e., the dimension having size unity in an a:b:1 model with a and b $\geq$ 1). Figure 14 contains plots of $(f_o/V_e)^{2\nu-1}$ with ν set to 1.5. Thus, 10^{-8} corresponds to a spatial-filter cutoff of 10 km and 10^{-6} to a cutoff of 1 km.

What we see in Figure 14 is that the detrender cutoff is at higher spatial frequencies in the isotropized spectrum, for all models, at Kwajalein than at Poker Flat. (That is, all calculated points lie above a 45° radial.) The small difference for isotropic (1:1) irregularities results from simple projection effects having to do with the different look angles to the satellite for the two data sets.

The dotted diagonal line in the lower portion of the figure corresponds to the isolated observational data point in Figure 12. That is, a model that produces a point on that line satisfies both observations. Again, there is no reason to expect a single model to satisfy both observations; the point is that all models except nearly isotropic ones result in effective spatial-filter cutoffs due to detrending that can readily explain the large disparity in the scintillation-index ratio for the two data sets.

3. Discussion

It is intuitively understandable that detrender action can affect the scintillation-index ratio because it directly sets the high-pass cutoff of phase scintillation, whereas the diffraction process itself performs that function for intensity scintillation, by means of Fresnel filtering. Thus, it was suspected a priori that the detrender, coupled with irregularity anisotropy and line-of-sight scanning, might play a role in the differences observed in the scintillation-index ratio at different stations. Figure 14 shows that the suspected effect is in the correct sense to explain the observation and is very strong.

Indeed, virtually all field-aligned models produce sufficiently anisotropic effective

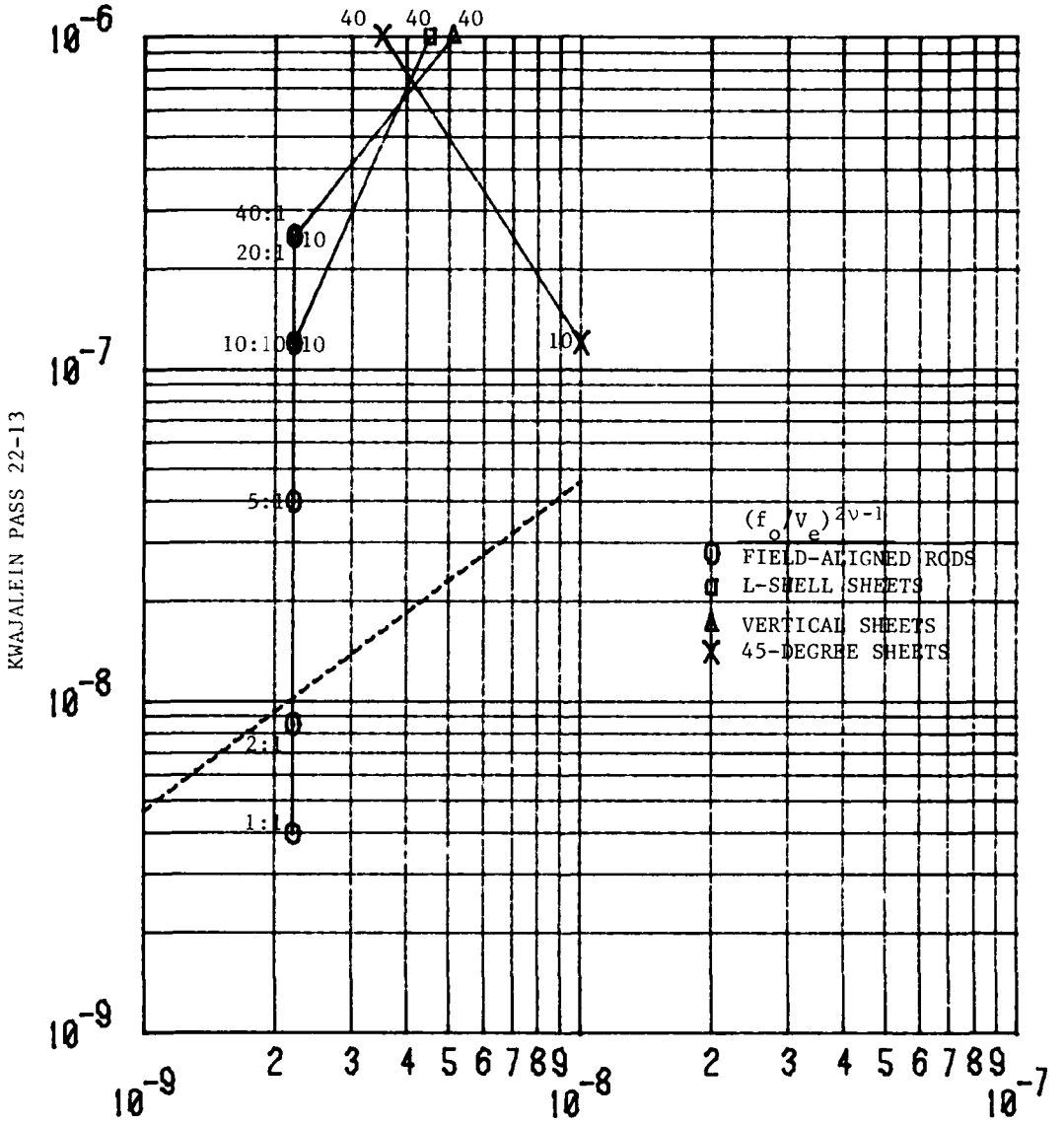

Figure 14. The factor $(f_o/V_e)^{2\nu-1}$ which arises from spatial filtering of anisotropic irregularities by means of the Wideband detrender. Dashed diagonal line in lower portion of figure corresponds to observed data point in Figure 12.

spatial-filter cutoffs that other factors must be operating to prevent even greater disparity in the index ratio observed at equatorial stations and at an auroral-zone location (for a high-inclination satellite such as Wideband). One such factor is the static diffraction factor represented by F/G. Another may be less steep irregularity spectra at auroral than at equatorial locations.

The result of this analysis underscores the central role played by a steep, effectively low-pass spatial spectrum of irregularities in dictating the signal statistics of scintillation. That is, since the outer scale of ionospheric structure lies outside the spectral window of structures that produce scintillation, an effective outer scale is imposed by the act of phase detrending.

The pertinent point is that the outer scale imposed is geometry-dependent. The result is that the Fresnel distance (ratio of Frensel-zone size to effective outer scale) depends strongly on the direction of scan relative to elongation axes of refractive-index structure. Detrending, therefore, reintroduces the concepts of "near" and "far" zones which appear to be lost in a strict power-law spectral environment. The relative efficacy of log-normal (near-zone) and generalized-Gaussian (far-zone) complex-signal statistics at various stations and different frequencies may be understood in these terms.

In closing this section, we stress that detrending effects are not to be viewed merely as artifacts of the Wideband experiment. Such effects arise in all experiments and operational systems, and they are important factors in controlling the quantitative relationship between phase and intensity scintillation and, therefore, the statistics of complex-signal scintillation.

IV. CONCLUSION

The Wideband experiment offers a good deal of insight into the behavior of signals that have undergone narrow-angle forward scattering in a random medium. From the present work, one may state several conclusions about the underlying statistics by which such signals may be described. First, both of the classical views -- ie, "multiplicative" and "additive" (Strohbehn, Wang, and Speck, 1975) -- contain elements of applicability to complex-signal statistics.

The multiplicative view, however, is appropriate only for describing phase fluctuations and weak intensity scintillation. Phase is nearly always normally distributed without regard to the strength of scatter or size of the Fresnel zone. Thus, its first-order statistics are altered very little by post-scattering propagation, caveats being that sufficient signal strength be maintained that phase remains defined and that the signal be sampled frequently enough that phase ambiguities are resolved.

Regarding intensity, the present analysis consistently supports the additive view. That is, the log-normal distribution for intensity is efficacious only in circumstances where there is little difference between it and other distributions (small Fresnel zone and/or weak scatter) or, occasionally, in situations where statistical significance is limited by lack of stationarity.

A strong conclusion can be made in favor of the Nakagami-m distribution for describing intensity scintillation. Often regarded as equivalent to the Rice distribution over the range of m usually encountered under scintillation conditions, the Nakagami distribution actually is an approximation to a more general intensity distribution consistent with the generalized Gaussian (additive) hypothesis. (cf, Section 3.1 (b) of Nakagami, 1960.) The Rice distribution was not tested specifically in this work, but the Nakagami distribution was found to be consistently efficacious over the range of m in which the two are somewhat different.

The conclusions quoted above lead to a suggestion that complex-signal statistics could be described very well by a bivariate distribution for intensity and phase that would reduce to the product of the Nakagami-m distribution and the normal distribution, respectively, when correlation between the variates is zero. In general, however, non-zero correlation is observed experimentally and is calculable from propagation theory. It is suggested that an inductive procedure starting from the Nakagami and normal distributions and invoking the necessary bivariate normalization might lead to a simple and efficacious model for complex-signal statistics that would adequately describe correlation between intensity and phase.

At present, only two-component hybrid models are able to provide a full description of

complex-signal statistics. The two-component model of Fremouw, Rino, and Livingston (1976), tested in this work, provides a valid description of complex-signal behavior for all relevant regimes of scattering strength and Fresnel-zone size. It does so, however, at the expense of requiring six parameters for its specification. A model based on the Nakagami and normal distributions, as suggested in the foregoing paragraph, would require only three parameters. For applications not requiring the joint statistics of (correlated) intensity and phase, the Nakagami-m and normal distributions can provide very efficacious descriptions on the basis of a single measured parameter each ($m = S_4^{-2}$ and σ_ϕ, respectively).

The two-component model yields insight into the physical processes governing signal behavior, in that it provides a basis for isolating effects adequately described by means of ray optics and effects dominated by diffractive scatter. In the model, these components are taken to obey log-normal and generalized Gaussian statistics, respectively. It is only in this context that generalized Gaussian statistics provide a (partial) description of complex-signal scintillation. Thus, while intensity scintillations are well described by distributions based on the generalized-Gaussian hypothesis, as was found by Rino, Livingston, and Whitney (1976) and as is totally consistent with the efficacious performance of the Nakagami-m distribution found in the present work, that hypothesis is not supported by, nor does it adequately describe, complex-signal scintillation.

In a strict sense, the data employed in this analysis describe signal behavior only in the "intermediate" zone, in which the Fresnel-zone radius lies between the inner and outer scales of a medium described by a power-law spatial spectrum. In principal, the inner scale was effectively zero (smaller than the spatial sampling size and/or lying at a point in the spatial spectrum that was dominated by noise) and the outer scale was effectively infinite (larger than the largest scale admitted in a data segment). Application of a detrending filter to the measured phase, however, had the effect of imposing an outer scale and allowed investigation of near-zone and far-zone behavior. Such investigation was facilitated, also, by the multi-frequency nature of the Wideband experiment.

Temporal detrending in the presence of highly anisotropic scatterers results in different imposed outer scales for different observing geometries -- in particular, for those encountered in observation of a high-inclination satellite from stations located at low, middle, and high latitudes. Such detrending, which is imposed in some fashion in nearly all measurements and applications, has a strong effect on the observed ratio of S_4 to σ_ϕ and, thereby, on the statistical behavior of the complex signal. This strong geometrical control over the relationship between intensity and phase statistics must be taken into account in any application dealing with total variances of refractive-index structure and/or signal fluctuations (as contrasted with power spectral densities of these same random variables).

LIST OF REFERENCES

Abramowitz, M. and I. A. Stegun (1964), Handbook of Mathematical Functions, Nat. Bur. Stds., Washington, D.C.

Barabenenkov, Yu. N., Yu. A. Kravtsov, S. M. Rytov, and V. I. Tamarskii (1971), "Status of the Theory of Propagation of Waves in a Randomly Inhomogeneous Medium", Uspekhi, Soviet Physics, 13,(5), 551-680.

Beard, C. I., W. T. Kreiss, and W. G. Tank, (1969), "A Multiwavelength Line-of-Sight Experiment for Remote Atmospheric Sensing", Proc. IEEE, 57, 446-458.

Beckman, P. and A. Spizzichino (1963), "The Scattering of Electromagnetic Waves from Rough Surfaces", Pergamon Press, New York, N. Y.

Booker, H. G., J. A. Ratcliffe, and D. H. Shinn (1950), "Diffraction from an Irregular Screen with Applications to Ionospheric Problems", Phil. Trans Roy Soc., A242, 579-607.

Bowhill, S. A. (1961), "Statistics of a Radio Wave Diffracted by a Random Ionosphere", J. of Res. Nat. Bur. of Stds., 65D, 275-292.

Bramley, E. N. (1955), "Some Aspects of the Rapid Directional Fluctuations of Short Radio Waves Reflected at the Ionosphere", Proc. IEEE, 102, 533-540.

Buckley, R. (1975), "Diffraction by a Random Phase-Changing Screen: A Numerical Experiment", J. Atmos. and Terres. Phys., 37, 1431-1446.

Crane, R. K. (1976), "Spectra of Ionospheric Scintillation", J. Geophys. Res., 81, 2041-2050.

de Wolf, D. A. (1969), "Are Strong Irradiance Fluctuations Log Normal or Rayleigh Distributed?", J. Opt. Soc. of America, 59(11), 1455-1460.

de Wolf, D.A. (1972), "Strong Amplitude Fluctuations of Wave Fields Propagating Through Turbulent Media", NTIS, US Dept. of Commerce, Springfield, VA, 22151.

de Wolf, D. A. (1975), "Propagation Regimes for Turbulent Atmospheres", Rad. Sci., 10(1). 53-57.

Dyson, P. L., J. P. McClure, and W. B. Hanson (1974), "In Situ Measurements of the Spectral Characteristics of F Region Ionospheric Irregularities", J. Geophys. Res., 79(10), 1497-1502.

Fante, R. L. (1975), "Electromagnetic Beam Propagation in Turbulent Media", Proc. IEEE, 63(12), 1669-1692.

Fremouw, E. J. (1978a), "Analysis of Wideband Satellite Data", Bimonthly Progress Report No. 1, Physical Dynamics Project 77-130, Contract DNA001-78-C-0042, Physical Dynamics, Inc., Bellevue, WA, 98009.

LIST OF REFERENCES (Continued)

Fremouw, E. J. (1978b), "*Analysis of Wideband Satellite Data*", Bimonthly Progress Report No. 2, Physical Dynamics' Project 77-130, Contract DNA001-78-C-0042, Physical Dynamics, Inc., Bellevue, WA 98009.

Fremouw, E. J. and J. M. Lansinger (1968), "*Radio-Star Visibility Fades in Alaska Near Solar Minimum*", J. Geophys. Res., 73, 3565-3572.

Fremouw, E. J. and J. M. Lansinger (1977), "*Examination of Data from the Wideband Satellite Experiment*", Final Progress Report, Physical Dynamics Project 118-R02, SRI Contract No. 14237, Physical Dynamics, Inc., Bellevue, WA 98009.

Fremouw, E. J., R. L. Leadabrand, R. C. Livingston, M. D. Cousins, C. L. Rino, B. C. Fair, and R. A. Long (1978), "*Early Results from the DNA Wideband Satellite Experiment -- Complex-Signal Scintillation*", Rad. Sci., 13(1), 167-187.

Fremouw, E. J. and R. C. Livingston (1976), "*Wideband Satellite Observations*", Bimonthly Progress Report 3, SRI Project 3793, Contract DNA001-75-C-0111, SRI International, Menlo Park, CA 94025.

Fremouw, E. J. and C. L. Rino (1975), "*Modeling of Transionospheric Radio Propagation*", Final Quarterly Tech. Report, SRI Project 3416, Contract No. F30602-74-C-0279, DARPA, SRI International, Menlo Park, CA 94025.

Fremouw, E. J. and C. L. Rino (1978), "*A Signal-Statistical and Morphological Model of Ionospheric Scintillation*", Proc. of AGARD Conference on Operational Modeling of the Aerospace Propagation Environment, Ottawa, Canada, 24-28 April.

Fremouw, E. J., C. L. Rino, and R. C. Livingston (1976), "*A Two Component Model for Scintillation*", presented at Cospar Beacon Satellite Group Symposium on "The Geophysical Use of Satellite Beacon Observations", 1-4 June, Boston University, MA.

Fremouw, E. J., C. L. Rino, R. C. Livingston, and M. C. Cousins (1977), "*A Persistent Subauroral Scintillation Enhancement Observed in Alaska*". Geophys. Res. Ltt., 4(11), 539-542.

Furuhama, Y. and M. Fukushima (1973), "*Measurements of the Log-Irradiance Distribution of a Laser Wave Propagated Through the Turbulent Atmosphere*", Boundary-layer Meteorol., 4, 433-477.

Gurvich, A. S. and V. I. Tatarskii (1975), "*Coherence and Intensity Fluctuations of Light in the Turbulent Atmosphere*", Rad. Sci., 10(1), 3-14.

Hajkowicz, L. A. (1978), private communication.

Hatfield, V. E. and C. L. Rino (1975), "*Non-Rician Statistics and Their Implications for Modeling Effects of Scintillation on Communication Channels*", in The Effect of the Ionosphere on Space Systems and Communications, J. M. Goodman, ed., NRL, Washington, D.C.

Hewish, A. (1951), "*The Diffraction of Radio Waves in Passing Through a Phase-Changing Ionosphere*", Proc. Roy. Soc. A., 209, 81.

LIST OF REFERENCES (Continued)

Ishimaru, A. (1975), "*Correlation Functions of a Wave in a Random Distribution of Stationary and Moving Scatterers*", (ed.) Rad. Sci., 10(1), 54-52.

Knepp, D. L. and G. C. Valley (1978), "*Properties of Joint Gaussian Statistics*", Rad. Sci., 13(1), 59-68.

Lovelace, R. V. E., E. E. Salpeter, L. E. Sharp, and D. E. Harris (1970), "*Analysis of Observations of Interplanetary Scintillations*", Astrophys. J., 159, 1047.

Mercier, R. P. (1962) "*Diffraction by a Screen Causing Large Random Phase Fluctuations*", Proc. Cambridge Phil. Soc., 58, 382-400.

Nakagami, M. (1960), "*The M-Distribution: A General Formula of Intensity Distribution of Rapid Fading*", Statistical Methods in Radio Propagation, edited by W. C. Hoffman, Pergamon Press, New York.

Ochs, G. R., R. R. Bergman, and J. R. Snyder (1969), "*Laser-Beam Scintillation Over Horizontal Paths from 5.5 to 145 Kilometers*", J. Opt. Soc. Amer., 59, 231-234.

Rice, S. O. (1945), "*Mathematical Analysis of Random Noise*", Part III, Bell Syst. Tech. J., 24(1), 47-159.

Rino, C. L. (1976), "*Ionospheric Scintillation Theory - A Mini-Review*", IEEE Trans. Antennas and Propagation, November.

Rino, C. L. and E. J. Fremouw (1977), "*The Angle Dependence of Single Scattered Wavefields*", J. Atmos. Terr. Phys., 39, 859-868.

Rino, C. L., R. C. Livingston, M. D. Cousins, B. C. Fair, and M. J. Baron (1978), "*Amplitude of Phase Scintillation at High and Equatorial Latitudes as Measured by the DNA Wideband Satellite*", Proc. 1978 Sym. on Effect of the Ionosphere on Space and Terrestrial Systems, NRL and ONR, Washington, D.C.

Rino, C. L., R. C. Livingston, and H. E. Whitney (1976), "*Some New Results on the Statistics of Radio Wave Scintillation: 1. Empirical Evidence for Gaussian Statistics*", J. Geophys. Res., 81(13), 2051-2057.

Rino, C. L. and S. J. Matthews (1978), "*On the Interpretation of Ionospheric Scintillation Data Using a Power-Law Phase Screen Model -- Weak Scatter*", Tech. Report 2, SRI Project 6434, Contract DNA001-77-C-0220, SRI International, Menlo Park, CA 94025.

Rytov, S. M. (1937), "*Diffraction of Light by Ultrasound Waves*", Izvestiya AN SSSR, Seriya Fizicheskaya, No. 2:223.

Salpeter, E. E. (1967), "*Interplanetary Scintillation. I. Theory*", Ap. J., 147(2), 433-449.

Singleton, D. G. (1970), "*Saturation and Focusing Effects in Radio-Star and Satellite Scintillations*", J. Atmos. Terres. Phys., 32, 187-208.

LIST OF REFERENCES (Continued)

Strohbehn, J. W. (1968), *"Line-of-Sight Wave Propagation Through the Turbulent Atmosphere"*, Proc. IEEE, 56(8), 1301-1318.

Strohbehn, J. W. and T. I. Wang (1972), *"Simplified Equation for Amplitude Scintillations in a Turbulent Atmosphere"*, Opt. Soc. Amer., 62(9), 1061-1068.

Strohbehn, J. W., T. I. Wang, and J. P. Speck (1975), *"On the Probability Distribution of Line-of-Sight Fluctuations of Optical Signals"*, Rad. Sci., 10(1), 59-70.

Tatarskii, V. I. (1971), *"The Effects of the Turbulent Atmosphere on Wave Propagation"*, NTIS, Springfield, VA.

Tsunoda, R. T., M. J. Baron, and J. Owen (1978), *"Altair: An Incoherent Scatter Radar for Equatorial Spread-F Studies"*, Top. Report for Period 1 June 1977 to 1 January 1978, SRI Project 6434, Contract DNA001-77-C-0220, DNA 4538T, DNA, Washington, D.C.

Uscinski, B. J. (1967), *"The Probability Distribution of the Wave Field Scattered by an Irregular Medium"*, J. Atmos. Terr. Phys, 29, 641-650.

Valley, G. C. and D. L. Knepp (1976), *"Application of Joint Gaussian Statistics to Interplanetary Scintillation"*, J. Geophys. Res., 81, 4723-4730.

Wang, T. I. and J. W. Strohbehn (1974a), *"Log-Normal Paradox in Atmospheric Scintillations"*, J. Opt. Soc. Amer., 64(5), 583-591.

Wang, T. I. and J. W. Strohbehn (1974b), *"Perturbed Log-Normal Distribution of Irradiance Fluctuations"*, J. Opt. Soc. Amer., 64(7), 994-999.

Whitney, H. E. (1974), *"Notes on the Relationship of Scintillation Index to Probability Distributions and Their Uses for System Design"*, Envirn. Res. Papers No. 461, Rep. No. AFCRL-TR-74-0004, IPL, AF Cambridge Res. Labs., L. G. Hanscom Field, Bedford, MA.

Whitney, H. E. and Santimay Basu (1977), *"The Effects of Ionospheric Scintillation on VHF/UHF Satellite Communications"*, Rad. Sci., 12, 123-133.

Yeh, K. C. (1972), *"Propagation of Spherical Waves Through an Ionosphere Containing Anisotropic Irregularities"*, J. Res. Nat. Bur. Stand., Sect. D. 66D, 621-636.

DISTRIBUTION LIST

DEPARTMENT OF DEFENSE

Assistant Secretary of Defense
Comm., Cmd., Cont. & Intell.
ATTN: C3IST&CCS, M. Epstein
ATTN: Dir. of Intelligence Systems,
J. Babcock

Assistant to the Secretary of Defense
Atomic Energy
ATTN: Executive Assistant

Command & Control Technical Center
ATTN: C-312, R. Mason
ATTN: C-650, G. Jones
3 cy ATTN: C-650, W. Heidig

Defense Advanced Rsch. Proj. Agency
ATTN: TIO

Defense Communications Agency
ATTN: Code R1033, M. Raffensperger
ATTN: Code 480, F. Dieter
ATTN: Code 101B
ATTN: Code 810, J. Barna
ATTN: Code 205
ATTN: Code 480

Defense Communications Engineer Center
ATTN: Code R410, J. McLean
ATTN: Code R720, J. Worthington
ATTN: Code R123
ATTN: Code R410, R. Craighill

Defense Intelligence Agency
ATTN: DB-4C, E. O'Farrell
ATTN: DB, A. Wise
ATTN: DT-5
ATTN: DC-7D, W. Wittig
ATTN: DT-1B
ATTN: HQ-TR, J. Stewart

Defense Nuclear Agency
ATTN: DDST
ATTN: STVL
3 cy ATTN: RAAE
4 cy ATTN: TITL

Defense Technical Information Center
12 cy ATTN: DD

Field Command
Defense Nuclear Agency
ATTN: FCPR

Field Command
Defense Nuclear Agency
Livermore Division
ATTN: FCPRL

Interservice Nuclear Weapons School
ATTN: TTV

Joint Chiefs of Staff
ATTN: C3S
ATTN: C3S, Evaluation Office

DEPARTMENT OF DEFENSE (Continued)

Joint Strat. Tgt. Planning Staff
ATTN: JLTW-2
ATTN: JPST, G. Goetz

National Security Agency
ATTN: R-52, J. Skillman
ATTN: B-3, F. Leonard
ATTN: W-32, O. Bartlett

Undersecretary of Defense for Rsch. & Engrg.
ATTN: Strategic & Space Systems (OS)

WWMCCS System Engineering Org.
ATTN: R. Crawford

DEPARTMENT OF THE ARMY

Assistant Chief of Staff for Automation & Comm.
Department of the Army
ATTN: DAAC-ZT, P. Kenny

Atmospheric Sciences Laboratory
U.S. Army Electronics R&D Command
ATTN: DELAS-EO, F. Niles

BMD Systems Command
Department of the Army
2 cy ATTN: BMDSC-HW

Deputy Chief of Staff for Ops. & Plans
Department of the Army
ATTN: DAMO-RQC

Electronics Tech. & Devices Lab.
U.S. Army Electronics R&D Command
ATTN: DELET-ER, H. Bomke

Harry Diamond Laboratories
Department of the Army
ATTN: DELHD-N-RB, R. Williams
ATTN: DELHD-N-P
ATTN: DELHD-N-P, F. Wimenitz
ATTN: DELHD-I-TL, M. Weiner

U.S. Army Comm.-Elec. Engrg. Instal. Agency
ATTN: CCC-EMEO-PED, G. Lane
ATTN: CCC-CED-CCO, W. Neuendorf
ATTN: CCC-EMEO, W. Nair

U.S. Army Communications Command
ATTN: CC-OPS-WR, H. Wilson
ATTN: CC-OPS-W

U. S. Army Communications R&D Command
ATTN: DRDCO-COM-RY, W. Kesselman

U.S. Army Foreign Science & Tech. Ctr.
ATTN: DRXST-SD

U.S. Army Materiel Dev. & Readiness Cmd.
ATTN: DRCLDC, J. Bender

U.S. Army Nuclear & Chemical Agency
ATTN: Library

DEPARTMENT OF DEFENSE CONTRACTORS (Continued)

ESL, Inc.
ATTN: J. Roberts
ATTN: J. Marshall
ATTN: C. Prettie

Ford Aerospace & Communications Corp.
ATTN: J. Mattingley

General Electric Co.
ATTN: M. Bortner

General Electric Co.
ATTN: A. Steinmayer
ATTN: S. Lipson
ATTN: C. Zierdt

General Electric Co.
ATTN: F. Reibert

General Electric Company-TEMPO
ATTN: DASIAC
ATTN: D. Chandler
ATTN: T. Stevens
ATTN: M. Stanton
ATTN: W. Knapp

General Electric Tech. Services Co., Inc.
ATTN: G. Millman

General Research Corp.
ATTN: J. Garbarino
ATTN: J. Ise, Jr.

GTE Sylvania, Inc.
ATTN: M. Cross

HSS, Inc.
ATTN: D. Hansen

IBM Corp.
ATTN: F. Ricci

University of Illinois
ATTN: Security Supervisor for K. Yeh

Institute for Defense Analyses
ATTN: H. Wolfhard
ATTN: J. Aein
ATTN: J. Bengston
ATTN: E. Bauer

International Tel. & Telegraph Corp.
ATTN: Technical Library
ATTN: G. Wetmore

JAYCOR
ATTN: S. Goldman

JAYCOR
ATTN: D. Carlos

Johns Hopkins University
ATTN: J. Newland
ATTN: Document Librarian
ATTN: T. Evans
ATTN: B. Wise
ATTN: P. Komiske
ATTN: T. Potemra

DEPARTMENT OF DEFENSE CONTRACTORS (Continued)

Kaman Sciences Corp.
ATTN: T. Meagher

Linkabit Corp.
ATTN: I. Jacobs

Litton Systems, Inc.
ATTN: R. Grasty

Lockheed Missiles & Space Co., Inc.
ATTN: R. Johnson
ATTN: W. Imhof
ATTN: M. Walt

Lockheed Missiles & Space Co., Inc.
ATTN: Dept. 60-12
ATTN: D. Churchill

M.I.T. Lincoln Lab.
ATTN: D. Towle
ATTN: L. Loughlin

McDonnell Douglas Corp.
ATTN: N. Harris
ATTN: W. Olson
ATTN: G. Mroz
ATTN: J. Moule

Mission Research Corp.
ATTN: R. Bogusch
ATTN: S. Gutsche
ATTN: D. Sowle
ATTN: F. Fajen
ATTN: R. Hendrick

Mitre Corp.
ATTN: G. Harding
ATTN: C. Callahan
ATTN: B. Adams
ATTN: A. Kymmel

Mitre Corp.
ATTN: W. Hall
ATTN: M. Horrocks
ATTN: W. Foster

Pacific-Sierra Research Corp.
ATTN: E. Field, Jr.

Pennsylvania State University
ATTN: Ionospheric Research Lab.

Photometrics, Inc.
ATTN: I. Kofsky

Physical Dynamics, Inc.
ATTN: D. Miller
5 cy ATTN: E. Fremouw

R & D Associates
ATTN: B. Yoon
ATTN: L. Delaney

Rand Corp.
ATTN: E. Bedrozian
ATTN: C. Crain

DEPARTMENT OF THE ARMY (Continued)

U.S. Army Satellite Comm. Agency
ATTN: Document Control

U.S. Army TRADOC Systems Analysis Activity
ATTN: ATAA-TDC
ATTN: ATAA-PL
ATTN: ATAA-TCC, F. Payan, Jr.

DEPARTMENT OF THE NAVY

Joint Cruise Missile Project Office
Department of the Navy
ATTN: JCM-G-70

Naval Air Development Center
ATTN: Code 6091, M. Setz

Naval Air Systems Command
ATTN: PMA 271

Naval Electronic Systems Command
ATTN: PME 106-13, T. Griffin
ATTN: PME 117-20
ATTN: PME 117-2013, G. Burnhart
ATTN: PME 117-211, B. Kruger
ATTN: PME 106-4, S. Kearney
ATTN: Code 3101, T. Hughes
ATTN: Code 501A

Naval Intelligence Support Ctr.
ATTN: NISC-50

Naval Ocean Systems Center
ATTN: Code 532, J. Bickel
ATTN: Code 5322, M. Paulson
3 cy ATTN: Code 5324, W. Moler

Naval Research Laboratory
ATTN: Code 7550, J. Davis
ATTN: Code 6780, S. Ossakow
ATTN: Code 6700, T. Coffey
ATTN: Code 7500, B. Wald

Naval Space Surveillance System
ATTN: J. Burton

Naval Surface Weapons Center
ATTN: Code F31

Naval Surface Weapons Center
ATTN: Code F-14, R. Butler

Naval Telecommunications Command
ATTN: Code 341

Office of Naval Research
ATTN: Code 420
ATTN: Code 421

Office of the Chief of Naval Operations
ATTN: OP 981N
ATTN: OP 941D
ATTN: OP 604C

Strategic Systems Project Office
Department of the Navy
ATTN: NSP-2722, F. Wimberly
ATTN: NSP-43
ATTN: NSP-2141

DEPARTMENT OF THE AIR FORCE

Aerospace Defense Command
Department of the Air Force
ATTN: DC, T. Long

Air Force Avionics Laboratory
ATTN: AAD, W. Hunt
ATTN: AAD, A. Johnson

Air Force Geophysics Laboratory
ATTN: LKB, K. Champion
ATTN: OPR-1, J. Ulwick
ATTN: PHP, J. Mullen
ATTN: OPR, A. Stair
ATTN: PHP, J. Aarons
ATTN: PHI, J. Buchau

Air Force Weapons Laboratory, AFSC
ATTN: DYC
ATTN: SUL

Air Logistics Command
Department of the Air Force
ATTN: OO-ALC/MM, R. Blackburn

Assistant Chief of Staff
Intelligence
Department of the Air Force
ATTN: INED

Assistant Chief of Staff
Studies & Analyses
Department of the Air Force
ATTN: AF/SASC, W. Adams
ATTN: AF/SASC, G. Zank

Ballistic Missile Office
Air Force Systems Command
ATTN: MNNL, S. Kennedy
ATTN: MNNH, M. Baran
ATTN: MNNH

Deputy Chief of Staff
Operations Plans and Readiness
Department of the Air Force
ATTN: AFXOKT
ATTN: AFXOKS
ATTN: AFXOKCD
ATTN: AFXOXFD

Deputy Chief of Staff
Research, Development, & Acq.
Department of the Air Force
ATTN: AFRDQ
ATTN: AFRDSS
ATTN: AFRDS
ATTN: AFRDSP

Electronic Systems Division
Department of the Air Force
ATTN: DCKC, J. Clark

Electronic Systems Division
Department of the Air Force
ATTN: XRW, J. Deas

Electronic Systems Division
Department of the Air Force
ATTN: YSEA
ATTN: YSM, J. Kobelski

DEPARTMENT OF THE AIR FORCE (Continued)

Foreign Technology Division
Air Force Systems Command
ATTN: NIIS Library
ATTN: SDEC, A. Oakes
ATTN: TQTD, B. Ballard

Headquarters Space Division
Air Force Systems Command
ATTN: SKA, M. Clavin
ATTN: SKA, C. Rightmyer

Headquarters Space Division
Air Force Systems Command
ATTN: SZJ, W. Mercer
ATTN: SZJ, L. Doan

Rome Air Development Center
Air Force Systems Command
ATTN: TSLD
ATTN: OCS, V. Coyne

Rome Air Development Center
Air Force Systems Command
ATTN: EEP

Strategic Air Command
Department of the Air Force
ATTN: DCX
ATTN: OOKSN
ATTN: DCXF
ATTN: XPFS
ATTN: DCXT
ATTN: NRT
ATTN: DCXT, T. Jorgensen

DEPARTMENT OF ENERGY CONTRACTORS

Lawrence Livermore Laboratory
ATTN: Document Control for Technical Information Dept. Library

Los Alamos Scientific Laboratory
ATTN: Document Control for P. Keaton
ATTN: Document Control for R. Taschek
ATTN: Document Control for D. Westervelt

Sandia Laboratories
ATTN: Document Control for Space Project Div.
ATTN: Document Control for D. Dahlgren
ATTN: Document Control for D. Thornbrough
ATTN: Document Control for 3141
ATTN: Document Control for Org. 1250, W. Brown

Sandia Laboratories
Livermore Laboratory
ATTN: Document Control for B. Murphy
ATTN: Document Control for T. Cook

OTHER GOVERNMENT AGENCIES

Central Intelligence Agency
ATTN: OSI/PSTD

Department of Commerce
National Bureau of Standards
ATTN: Sec. Officer for R. Moore

OTHER GOVERNMENT AGENCIES (Continued)

Department of Commerce
National Oceanic & Atmospheric Admin.
Environmental Research Laboratories
ATTN: R. Grubb

Institute for Telecommunications Sciences
National Telecommunications & Info. Admin.
ATTN: A. Jean
ATTN: D. Crombie
ATTN: L. Berry
ATTN: W. Utlaut

U.S. Coast Guard
Department of Transportation
ATTN: G-DOE-3/TP54, B. Romine

DEPARTMENT OF DEFENSE CONTRACTORS

Aerospace Corp.
ATTN: I. Garfunkel
ATTN: S. Bower
ATTN: N. Stockwell
ATTN: R. Slaughter
ATTN: D. Olsen
ATTN: F. Morse
ATTN: V. Josephson
ATTN: T. Salmi

University of Alaska
ATTN: N. Brown
ATTN: Technical Library
ATTN: T. Davis

Analytical Systems Engineering Corp.
ATTN: Radio Sciences

Analytical Systems Engineering Corp.
ATTN: Security

Barry Research Communications
ATTN: J. McLaughlin

BDM Corp.
ATTN: T. Neighbors
ATTN: L. Jacobs

Berkeley Research Associates, Inc.
ATTN: J. Workman

Boeing Co.
ATTN: D. Murray
ATTN: S. Tashird
ATTN: G. Hall
ATTN: J. Kenney

Charles Stark Draper Lab, Inc.
ATTN: D. Cox
ATTN: J. Gilmore

Computer Sciences Corp.
ATTN: H. Blank

Comsat Labs
ATTN: R. Taur
ATTN: G. Hyde

Electrospace Systems, Inc.
ATTN: H. Logston

DEPARTMENT OF DEFENSE CONTRACTORS (Continued)

R & D Associates
ATTN: R. Turco
ATTN: F. Gilmore
ATTN: C. Greifinger
ATTN: W. Wright, Jr.
ATTN: C. MacDonald
ATTN: R. Lelevier
ATTN: W. Karzas
ATTN: M. Gantsweg
ATTN: H. Ory
ATTN: B. Gabbard

Riverside Research Institute
ATTN: V. Trapani

Santa Fe Corp.
ATTN: E. Ortlieb

Science Applications, Inc.
ATTN: L. Linson
ATTN: E. Straker
ATTN: D. Sachs
ATTN: J. McDougall
ATTN: D. Hamlin
ATTN: C. Smith

Science Applications, Inc.
ATTN: D. Divis

DEPARTMENT OF DEFENSE CONTRACTORS (Continued)

Science Applications, Inc.
ATTN: SZ

SRI International
ATTN: G. Smith
ATTN: W. Jaye
ATTN: D. Neilson
ATTN: R. Leadabrand
ATTN: W. Chesnut
ATTN: R. Livingston
ATTN: G. Price
ATTN: A. Burns
ATTN: M. Baron
ATTN: C. Rino

Teledyne Brown Engineering
ATTN: R. Deliberis

TRW Defense & Space Sys. Group
ATTN: D. Dee
ATTN: S. Altschuler
ATTN: R. Plebuch

Visidyne, Inc.
ATTN: J. Carpenter